

The structure, function and engineering of a thermostable nitrile hydratase



William Nyasha Mavengere

UNIVERSITY *of the*
WESTERN CAPE

A thesis submitted in partial fulfilment of the requirements for the degree of Magister Scientae in the
Department of Biotechnology, University of the Western Cape.

Supervisor: Prof D.A. Cowan

November 2008

ABSTRACT

The structure, function and engineering of a thermostable Nitrile Hydratase

William Nyasha Mavengere

MSc thesis, Department of Biotechnology, University of the Western Cape.

Nitrile hydratases (NHases) are enzymes that catalyse the conversion of organocyanides to amides via a non-hydrolytic hydration reaction. They are industrially relevant enzymes, currently used in the manufacture of nicotinamide and acrylamide. The target of this study belongs to the thermophilic bacteria *Geobacillus pallidus*. The *G. pallidus* RAPc8 NHase is a heterotetramer that has a 28 kDa α subunit and a 29 kDa β subunit, with a $\alpha_2\beta_2$ configured functional unit. The *G. pallidus* RAPc8 NHase operon has been cloned, sequenced and expressed at high levels in *E. coli*, with subsequent crystallisation for X-ray diffraction analysis. Current work is based on the study of the reaction mechanism of NHase as proposed by Mitra and Holz (2006). This mechanism implicated $\beta Y72$ and $\beta W76$ in the hydration of nitriles. The study involved the site directed mutation of the β subunit of *G. pallidus* RAPc8 NHase, resulting in the generation of a $\beta Y72F\beta W76V$ mutant. This was followed by sequencing, expression and purification of the recombinant protein. The pH-activity and temperature- activity profiles of the mutant showed the enzyme to be optimally active at pH 6.4 and 55°C, respectively. Further kinetic analysis of the mutant found optimal k_{cat}/K_M values of 94.7 ± 7.5 at 50°C and pH 5.8. The determination of the kinetic parameters under differing environmental conditions such as changes in temperature and pH revealed the ionisation constants of the enzyme-substrate complex (pK_{ES1} and pK_{ES2}) to be 5.9 and 7.7, respectively. These results suggest

that the active site sulphinic acid as opposed to the active site tyrosine may be responsible for catalysis. The active site tyrosine probably plays a substrate-stabilising role. The fluctuation of the k_{cat} , K_M and k_{cat}/K_M values demonstrated the need to use an alternative measure of enzyme efficiency. A more appropriate term could be the enzyme efficiency function, E_f , which considers the dependence of the enzyme efficiency on substrate concentration.



Declaration

I declare that *The structure, function and engineering of a thermostable Nitrile Hydratase* is my own work, that it has not been submitted before for any degree or examination in any other university, and that all the sources I have used or quoted have been indicated and acknowledged as complete references.

William N. Mavengere



November 2008

Signed:

Acknowledgements

I would like to thank all of the Research Students, Post doctoral fellows and Technical staff in the IMBM laboratory for their assistance. Special mention goes to my Supervisor Prof D.A. Cowan, for giving me the opportunity to do this degree, and Dr H. Goodman, for helping me “put out the fires”. Thanks to Dr M. Sayed of the Biotechnology department at the University of the Western Cape (SA), Prof R. Daniel of the University of Waikato (NZ), Prof T. Sewell of the University of Cape Town (SA), and Prof M. Danson of the University of Bath (UK). Your experience and knowledge was quintessential to the completion of this work. I would like to thank my family; my Mom, my sisters Lydia and Omega; my “vazukurus” (Leigh-Ann, Laura, Wilson and Davidzo), my “Tsanos” Ernest, Edward, and Shungu, my Parents-in-law, my Daughters Miriam and Deborah. I would also like to thank my most significant Professional Colleague, (who also happens to be the love of my life) Natasha. Without you, none of this could have been possible. To God be the glory!



To Mama, for the sacrifices.....
UNIVERSITY OF
WESTERN CAPE

Abbreviations

Alanine / Adenine /amps	A
Angstrom	Å
Alpha subunit cysteine suphinic acid	α CEA
Alpha subunit cysteine suphenic acid	α CSD
Serine residue from the alpha subunit	α SER
Bovine serum albumin	BSA
Cysteine / Cytosine	C
Aspartate	D
Dalton	Da
Glutamate	E
Efficiency function	E_f
Phenylalanine /Faraday	F
Glycine / Guanine/Gibbs free energy	G
Gram	g
Planck's constant ($6.6261 \times 10^{-34} \text{ Js}^{-1}$)	h
Isoleucine	I
Isopropyl -D-1-thiogalactopyranoside	IPTG
Incremental truncation for the creation of hybrid enzymes	ITCHY
Joule	J
Lysine / Kelvin	K
Boltzmann's constant ($1.3807 \times 10^{-23} \text{ JK}^{-1}$)	k_B
kilodalton	kDa



Michaelis-Menten constant	K_m
Leucine	L
Molar / Methionine	M
Asparagine	N
Nitrile Hydratase	NHase
Ohm	Ω
Proline	P
Polyacrylamide gel electrophoresis	PAGE
Polymerase chain reaction	PCR
Protein Data Bank	PDB
Glutamine	Q
Gas constant ($8.3145 \text{ JK}^{-1}\text{mol}^{-1}$) / Arginine	R
Random chimeragenesis on transient templates	RACHITT
Random priming recombination	RPR
Serine/Sulphur	S
Sodium dodecyl sulphate	SDS
Sequence homology-independent protein recombination	SHIPREC
Staggered extension process	StEP
Threonine / Thymine	T
Uracil	U
Valine / volts	V
Initial velocity	v
Maximum velocity	V_{\max}



Tryptophan

W

Tyrosine

Y

Termination codon

*



ABSTRACT.....	2
DECLARATION.....	4
ACKNOWLEDGEMENTS	5
ABBREVIATIONS	7
CHAPTER 1: INTRODUCTION.....	13
1.1 Distribution, biological role and applications of nitrile metabolising enzymes.....	13
Figure 1.1.1: Different pathways of nitrile metabolism	14
1.2 Distribution, biological role and applications of NHases	16
1.3 Molecular structure, activity and substrate specificity of NHases	18
Figure 1.3.1: Superimposition of the active sites of <i>Pseudomonas thermophila</i> JCM3095, a Co-type NHase (shown in blue) and <i>Rhodococcus sp.</i> N-771, an Fe-type NHase (shown in yellow)	19
1.4 Constituents of a NHase functional unit.....	20
Figure 1.4.1: Four possible mechanisms for the formation of the NHase dimer	20
Figure 1.4.2: Substrate channel of <i>G. pallidus</i> RAPc8 NHase.	22
Figure 1.4.3: Cobalt-binding site of NHase showing claw-setting motif. The α CSD119 and α CEA121 represent a sulphinic and sulphenic acids respectively (Tsekoo, 2005).	23
1.5 <i>G. pallidus</i> RAPc8 NHase RAPc8 operon	23
Figure 1.5.1: <i>G. pallidus</i> RAPc8 NHase gene cluster showing open reading frames	24
1.6 Enzyme redesign	26
Figure 1.6.1: Four strategies for redesigning enzyme functions	27
1.7 The reaction mechanism of NHases	29
Figure 1.7.1: Tyrosinate base reaction mechanism of NHase	29
Figure 1.7.2: Sulphinic base reaction mechanism of NHase	30
1.8 Rationale.....	31
Table 1.8.1: Kinetic constants of wild-type and the β W76G mutated NHase	31
Table 1.8.2: Kinetic values for <i>G. pallidus</i> RAPc8 NHase strains	33
CHAPTER 2: METHODOLOGY.....	34
Table 2.1 Composition of buffers and solutions	34
2.1 In silico procedures.....	35
Figure 3.3.1: DNA and amino acid sequences of the <i>G. pallidus</i> RAPc8 NHase β subunit.	36
2.2 Site-directed mutagenesis.....	37
2.3 Preparation and transformation of electrocompetent cells.....	38
2.5 Verification of transformation and mutagenesis success	40

2.6 Expression of the NHase mutants	41
2.7 Purification of NHase mutants	42
2.8 Enzyme kinetics	43

CHAPTER 3: THE ENGINEERING, EXPRESSION AND PURIFICATION OF *G. PALLIDUS* RAPc8 NHASE 46

3.1 Introduction	46
3.2 In silico procedures.....	47
Figure 3.2.1: Alignment of the molecular structures of <i>G. pallidus</i> RAPc8 NHase (2dpp) and <i>P. thermophila</i> NHase (1IRE).....	47
The ribbon diagram shows the heterodimers of the <i>P. thermophila</i> and <i>G. pallidus</i> RAPc8 NHase which are shown in blue and green respectively. The α subunits are shown in pale shades, whereas the β subunits are brightly coloured.....	47
Figure 3.2.2: Active site residues of the <i>G. pallidus</i> RAPc8 NHase.....	48
3.3 Site directed mutagenesis.....	49
Figure 3.3.1: Agarose gel of the PCR products.....	50
3.4 Protein purification and expression.....	51
Figure 3.4.1: Hydrophobic interaction chromatogram of the.....	51
Figure 3.4.2: Ion exchange chromatogram of the.....	52
Figure 3.4.3: Gel filtration chromatogram of the.....	53
Figure 3.4.4: Modified Bradford assay standard curve.....	54
Table 3.4.1: Purification table of the $\beta Y72F\beta W76V$ mutant NHase.....	54
Figure 3.4.5: SDS – PAGE gel of the.....	55
Figure 3.4.6: Standard curve of the logarithm of the molecular weight markers against the distance travelled on the SDS-PAGE gel.....	56

CHAPTER 4: KINETIC ANALYSIS OF THE $\beta Y72F\beta W76V$ MUTANT NHASE 57

4.1 Absorption spectra, calibration and preliminary assays.....	57
Figure 4.1.1: Absorption spectra for the NHase substrate and product.	57
Figure 4.1.2: Calibration curve for acrylamide at 225 nm.	58
Figure 4.1.3: Absorbance vs. time plot for 0.1 mg ml ⁻¹ of the $\beta Y72F\beta W76V$ mutant NHase.	59
4.2 Kinetic parameters of the $\beta Y72F\beta W76V$ mutant NHase.....	59
4.2.1 Michealis-Menten kinetics	59
Figure 4.2.1: Michealis-Menten curve for the mutant	60
Figure 4.2.2: Michealis constants of <i>G. pallidus</i> RAPc8 NHase mutants.....	61
4.2.2 Efficiency function: An alternative catalytic comparator.....	62
Table 4.2.2: Efficiency function values of three <i>G. pallidus</i> RAPc8 NHases.....	63
Figure 4.2.4: Efficiency function graph of the <i>G. pallidus</i> RAPc8 NHase mutants	63
Table 4.2.3: Specificity constants of the <i>G. pallidus</i> RAPc8 NHases mutants.....	64
4.3 Effect of temperature on the kinetic parameters of the <i>G. pallidus</i> RAPc8 $\beta Y72F\beta W76V$ mutant NHase.....	65
Table 4.3.1: Kinetic parameters of <i>G. pallidus</i> RAPc8 $\beta Y72F\beta W76V$ mutant NHase.....	65

4.3.1 TEMPERATURE DEPENDENCE OF K_{CAT}	65
4.3.2 Temperature dependence of K_m	67
4.3.3 Thermodynamic parameters of <i>G. pallidus</i> RAPc8 βY72FβW76V NHase	68
Table 4.3.2: Thermodynamic parameters of the <i>G. pallidus</i> RAPc8 β Y72F β W76V mutant, <i>C. testosteroni</i> (Rao and Holz, 2008) and <i>P. thermophila</i> (Mitra and Holz, 2006) NHase	68
4.3.4 Temperature dependence of k_{cat}/K_m	69
Table 4.3.3 Variation of the <i>G. pallidus</i> RAPc8 NHase β Y72F β W76V efficiency function with temperature	71
4.4 The effect of pH on the kinetic parameters	72
Figure 4.4.1 : pH-activity profile of the β Y72F β W76V mutant NHase	72
4.4.1 Enzyme Inhibition by MES buffer	73
4.4.2 pH dependence of kinetic parameters	74
Table 4.4.1: pH dependence of the kinetic parameters for <i>G. pallidus</i> RAPc8 β Y72F β W76V NHase....	74
Figure 4.4.2: log k_{cat} vs pH plots of <i>G. pallidus</i> RAPc8 NHase β Y72F β W76V with acrylonitrile as the substrate	75
Figure 4.4.4: log k_{cat} / K_m vs pH plot of the <i>G. pallidus</i> RAPc8 NHase β Y72F β W76V mutant with acrylonitrile as the substrate.	77
Table 4.4.2 Ionisation constants of the <i>G. pallidus</i> RAPc8 β Y72F β W76V mutant NHase.....	78
Table 4.4.3 Variation of the <i>G. pallidus</i> RAPc8 β Y72F β W76V mutant NHase efficiency function with pH	81
CHAPTER 5: GENERAL DISCUSSION AND CONCLUSIONS	82
5.1 Summary	82
5.2 Further studies	84
REFERENCES	87

Chapter 1: Introduction

Nitrile hydratases (NHases) are enzymes that catalyse the conversion of organocyanides to amides via a non-hydrolytic hydration of the cyanide bond. They are members of the nitrile metabolising enzymes (NMEs), together with nitrilases and amidases. NMEs are present in both prokarya and eukarya, playing a role in secondary bacterial metabolism with plant and fungal symbionts in particular. Their ability to modify organic compounds makes them candidates for biotechnological exploitation. The NHase under study belongs to the thermophilic bacteria *Geobacillus pallidus*, which has the potential of being an ideal biocatalyst in the production of important industrial chemicals such as acrylamide. The *G. pallidus* NHase operon has been cloned, sequenced and expressed at high levels in *E. coli*, with the subsequent crystallisation for X-ray diffraction analysis (Tsekoa *et al.*, 2004). The following is a review of literature pertaining to the further study of the structural and mechanistic basis of substrate specificity in *G. pallidus* NHase.

1.1 Distribution, biological role and applications of nitrile metabolising enzymes

Nitrilase metabolism is present in Graminiceae, Cruciferae and Musceae, three of the twenty one known plant families. It is also noted in the *Fusarium*, *Penicillium* and *Aspergillus* fungal genera (Cowan *et al.*, 1998). Cyanoglycosides, cyanolipids, ricinine and phenylacetone nitrile are examples of nitriles produced in plants (Banerjee *et al.*, 2002). Nitrilase and amidase reactions are responsible for the production of auxins (such as

indole-3-acetic acid), biotin, β -alanine and other natural products which result in amino acid deamination via cyano or carbonyl carbon attack by a conserved cysteine (Pace and Brenner, 2001).

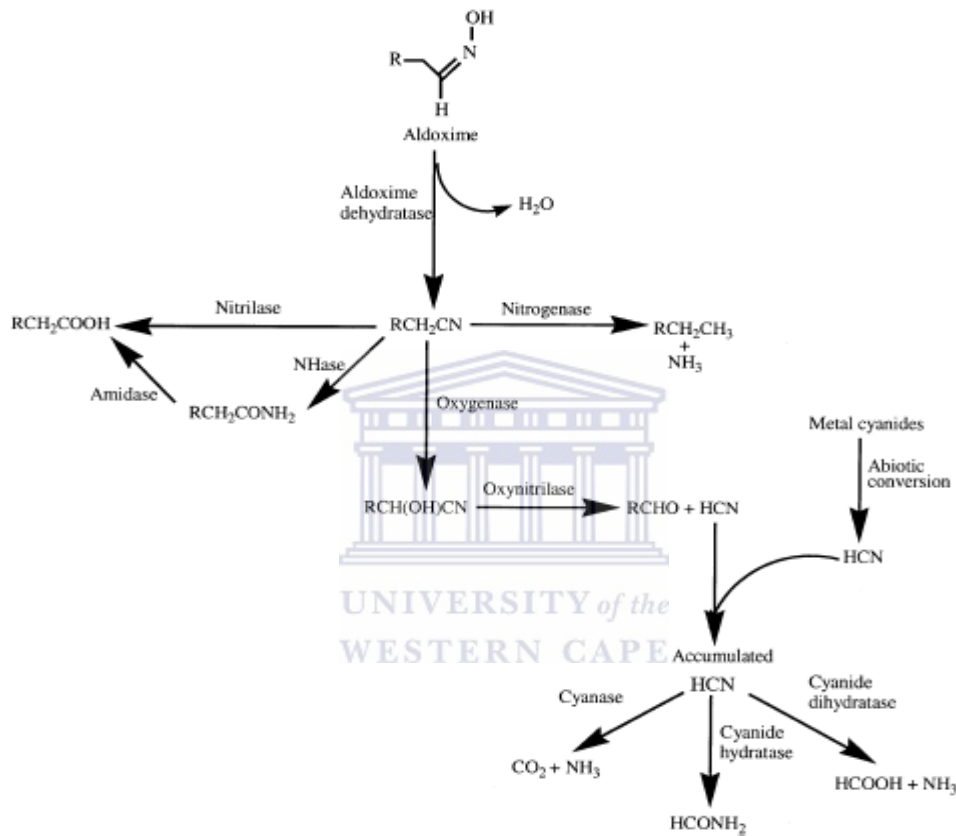


Figure 1.1.1: Different pathways of nitrile metabolism (Banerjee *et al.*, 2002)

Figure 1.1.1 shows the different pathways involved in plant nitrile metabolism. NHases have been shown to participate as catalysts in the metabolism of aldoximes. Aldoximes are a class of natural plant product intermediates, and aldoxime dehydratase is an enzyme

in the same gene cluster as NMEs and acyl CoA synthase (Tsekoa, 2005; Cameron *et al.*, 2005). The conversion of an aldoxime to a nitrile by aldoxime dehydratase, leads to the formation of a carboxylic acid either directly via nitrilase activity or through the action of NHase and amidase enzymes. Carboxylic acid may then be converted to acyl CoA, a carbon source, by a ligase enzyme (Kato and Aasano, 2006).

Synthetic nitriles are used in a variety of industrial processes. Acrylonitrile and adiponitrile are both required for the synthesis of polyacrylonitrile and nylon 66. Nitriles are used in the production of feedstock, solvents, extractants, drug intermediates (chiral synthons), and pesticides. They are intermediates in the synthesis of amines, amides, amidines, carboxylic acids, esters, aldehydes, ketones and heterocyclic compounds (Graham *et al.*, 2000; Banerjee *et al.*, 2002). Not all industrial by-products of nitrile synthesis are useful. Some become part of industrial effluent, finding their way into the environment with deleterious effects to living organisms. Nitriles are generally mutagenic and carcinogenic, having been implicated as the causative agent in conditions such as gastric problems, nausea, bronchial irritation, respiratory distress, convulsions, comas and osteolathrysm (Banerjee *et al.*, 2002). Nitriles inactivate the respiratory system by binding tightly to cytochrome-c-oxidase. Biological methods such as the use of NMEs could be used to remove such toxicants from the environment.

NME-expressing bacteria metabolise acrylonitrile, fumaronitrile, and succinonitrile to 99 % removal when grown in batch and continuous culture (Banerjee *et al.*, 2002). *Agrobacterium radiobacter* produces an NME that decreases 3, 5-dibromonitrile levels

by 65 % after five days of exposure (Banerjee *et al.*, 2002). Degradation can be enhanced by the addition of metal ions. *Geobacillus pallidus* is able to grow in aliphatic nitriles such as acetonitrile and valeronitrile, but not in aromatic nitriles such as benzonitrile. (Pereira *et al.*, 1998). It does not express benzonitrilase, an enzyme that degrades the aromatic nitrile benzonitrile (Pereira *et al.*, 1998). Isolation and recombinant expression of NME's would be preferred to the use of whole cell biocatalysts as there would be a conservation of resources and the prospect of reusability of the biocatalysts.

1.2 Distribution, biological role and applications of NHases

NHases are present in a variety of bacteria such as *Agrobacteria*, *Corynebacteria*, *Arthrobacteria*, *Pseudomonas* and *Rhodococcus*. These bacteria reside in diverse ecosystems such as terrestrial soils, thermal lake sediments and deep sea trenches (Graham *et al.*, 2000).

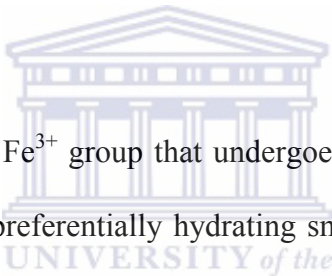
NHases can be used produce important chemicals such as acrylamide, as well as pharmaceuticals and biotechnologicals. They may also be used in organocyanide effluent treatment (Pereira *et al.*, 1998). Immobilised NHase producing microbes were used by the Mitsubishi-Rayon Chemical Company, a Japanese firm, to synthesise kilotonne levels of acrylamide. Nicotinamide, niacinamide and vitamin B₃ were produced by the Lonza Guangzhou Fine Chemicals Company in China, while DuPont produced 5-cyanovaleramide (5-CVAM), the starting material for the herbicide azafenidin (Cameron *et al.*, 2005). 5-CVAM is produced using Raney copper or MnO₂ catalyst at 130°C. This

method has the co-production of adipanide. *P. chloraphis* B23 is a regioselective biocatalyst, producing only 0.006 kg (waste) (kg)⁻¹(product) of 5-CVAM produced (Snell and Colby, 1998). D-phenylglycine amide is a β -lactam intermediate formed by *Rhodococcus sp.* from a racemic mixture of phenylglycine nitrile (Snell and Colby, 1998). 2-arylpropanoic acids such as ibuprofen are anti-inflammatory drugs. The (S) enantiomer of ibuprofen is more potent than the (R) enantiomer. *Rhodococcus sp.* AJ270 could be used for that reaction, as it has been found to preferentially produce the desired S enantiomer (Snell and Colby, 1998).

Instability at high temperatures and under chaotropic conditions has hindered the utilisation of NHase as biocatalysts in the industrial process. This is because most of the well characterised NHases are mesophilic in nature. They have been shown to be unstable in the absence of substrates or substrate analogues. This has implications as to the reusability of these NHases (Pereira *et al.*, 1998). Indeed, the possibility of employing more stable enzymes at higher operating temperatures or in the presence of denaturants such as organic solvents has led to the search for thermophilic homologues of mesophilic NHases.

1.3 Molecular structure, activity and substrate specificity of NHases

NHases (EC 4.2.1.84) are non-hydrolytic hydratase enzymes that are classified on the basis of their metal ion co-factor. The two predominant types are the non-haeme Fe- and the non-corrinoid Co-types. An exception to the rule is the *Myrothecium verrucaria* NHase which has a zinc co-factor (Cramp and Cowan, 1999). NHases share the co-factor binding motif CXLCS, where X designates serine (S) in Fe-type and threonine (T) in Co-type NHases (Cameron *et al.*, 2005). These metal ions are embedded in the active site to enhance polypeptide subunit stability and catalyse cyanide hydration (Banerjee *et al.*, 2002).



The Fe-type NHases possess a Fe^{3+} group that undergoes photo-induced denitrosylation by binding nitrous oxide, and preferentially hydrating small aliphatic nitriles (Periera *et al.*, 1998). Fe-type possesses two cysteine (C) residues coordinated to the Fe ion that are post-translationally modified to a C-sulphinic acid and a C-sulphenic acid, yielding a claw setting structure (Miyanga *et al.*, 2004). A proposed metal binding motif CXCC is essential for NHase activation in Fe-type (Cameron *et al.*, 2004).

Figure 1.3.1 shows an active site tryptophan (W72) residue in the *beta* (β) subunit of the *Pseudomonas thermophila* JCM3095 that is homologous to β W76 of *G. pallidus* RAPc8 NHase. It has been reported to be involved in substrate binding in Co-type NHases as opposed to a tyrosine (Y) residue in Fe-type. The Fe-type Y residue is homologous to β Y76 of *Rhodococcus sp.* N-771 (Miyanga *et al.*, 2001). The direction of the side chain

of W72 residue in Co-type NHases is different from that of the corresponding Y76 residue in Fe-type NHases. The β subunit leucine (L) and phenylalanine (F) residues (β L48 and β F51 in *P. thermophila* JCM3095) in Co-type NHases occupy the spatial position of the β Y side chain of Fe-type NHases. In Fe-type NHases, the L and F residues correspond to two β subunit valine (V) residues (β V52 and β V56 in *Rhodococcus sp.* N-771) (Miyanga *et al.*, 2001). These differences result in a larger surface area in the substrate binding site of Fe-type NHases, and possibly explaining the inability of Co-type NHases to metabolise aromatic and side chain possessing aliphatic nitriles. It suggests that substrate-binding pocket hydrophobicity is not the primary determinant of specificity (Pereira *et al.*, 1998).

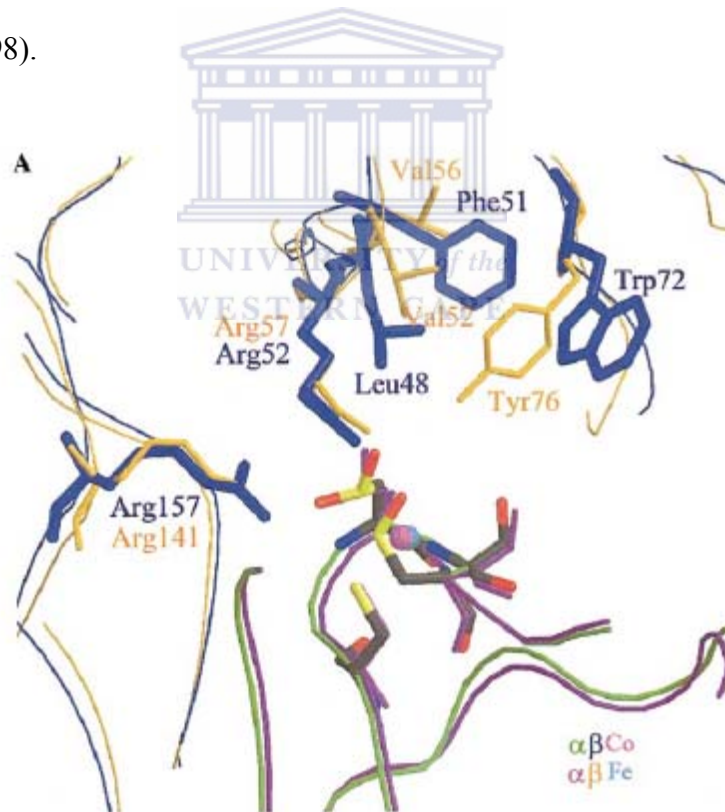


Figure 1.3.1: Superimposition of the active sites of *Pseudomonas thermophila* JCM3095, a Co-type NHase (shown in blue) and *Rhodococcus sp.* N-771, an Fe-type NHase (shown in yellow) (Miyanga *et al.*, 2001)

1.4 Constituents of a NHase functional unit

NHases are predominantly heterotetrameric (Pereira *et al.*, 1998), though exceptions such as the dimeric *Agrobacterium tumefaciens* and *Corynebacterium* CS, as well as the monomeric *Rhodococcus equi* NHases do exist (Miyanga *et al.*, 2001). The α and β subunits are coded for by two separate but adjacent open reading frames (ORFs) (Cameron *et al.*, 2005). The *G. pallidus* RAPc8 NHase has a 28 kDa α subunit and a 29 kDa β subunit having a $\alpha_2\beta_2$ configured functional unit (Pereira *et al.*, 1998). There are four possible mechanisms for the assembly of the dimer, as shown in Figure 1.4.1 below. Mechanism D is believed to be the most likely mechanism. It shows the initial formation of a α subunit-P14k complex, which binds a Co ion. Then, the p14k accessory protein facilitates the association the β subunit and of its dissociation from the complex.

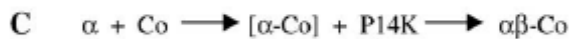
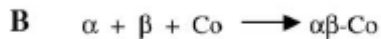
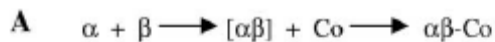


Figure 1.4.1: Four possible mechanisms for the formation of the NHase dimer (Cameron *et al.*, 2005)

The 30 amino acid-residue β subunit wraps around the α subunit, with the Co at the interface, highlighting the significance of the stabilisation and orientation of dimer interaction (Pereira *et al.*, 1998). The globular domain of the α subunit is nestled in the groove-like region between the α helix domain and the β sheet domain of the β subunit. This globular domain interacts with amino acids from both domains of the β subunit (Tsekoo, 2005).

The α subunit has a protruding N-terminal arm comprising 3 α -helices. The 3 α -helices are separated by a large globular domain that consists of 9 α -helices and 4 β -strands (Tsekoo., 2005). The β subunit has two distinct domains. The N-terminus begins with a long loop interrupted by a short α -helix. The loop leads to a domain that is composed of 7 α -helices. The second domain is comprised of two small α -helices, two small β -strands and a prominent anti-parallel β -sheet formed from four strands.

G. pallidus RAPc8 NHase surface analysis revealed an extended, curved substrate channel (active-site entry channel) with access to bulk solvent from two locations in the heterodimer, as shown in Figure 1.4.2 below. This channel lies at the interface between the α and β subunits of NHase and traverses past the metal binding site. (Lang *et al.*, 1998). The channel is clearly localised at the interface between the α and β subunits.

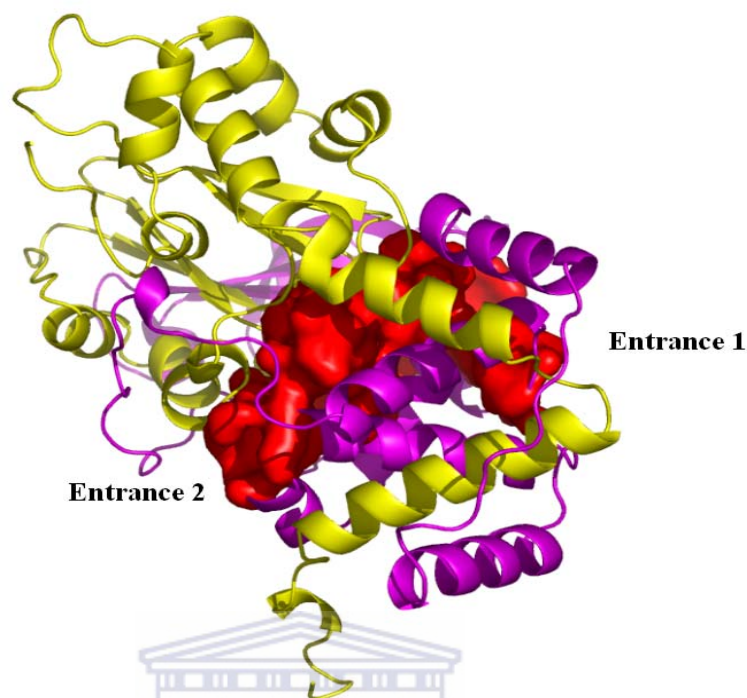


Figure 1.4.2: Substrate channel of *G. pallidus* RAPc8 NHase.

The major pocket was identified using CASTp. This pocket was designated as the substrate channel of NHase. (Yellow: α subunit, purple: β subunit, red: substrate channel).

All known NHases exhibit a highly homologous amino acid sequence; 3 cysteine (C) residues and a serine (S) residue in that cluster region, coordinating the metal ion of the α subunit, and 2 arginine (R) residues of the β subunit (Miyanga *et al.*, 2004). The presence of the modified cysteine residues that form the claw-setting motif at the active site among the channel-forming residues provides some confidence in the designation as the substrate channel. This claw setting motif is highlighted in Figure 1.4.3. The Co-type NHase metal ion forms an octahedral coordination complex, with amino acids α C119, α S120, and α C121 on the vertices of the octahedral vertices. NHases undergo post-

translational modification of the α C119 and α C121 residues (Hourai *et al.*, 2003), which are oxidised to a sulphenic acid and a sulphonic acid, respectively as shown in figure 1.4.3 below.

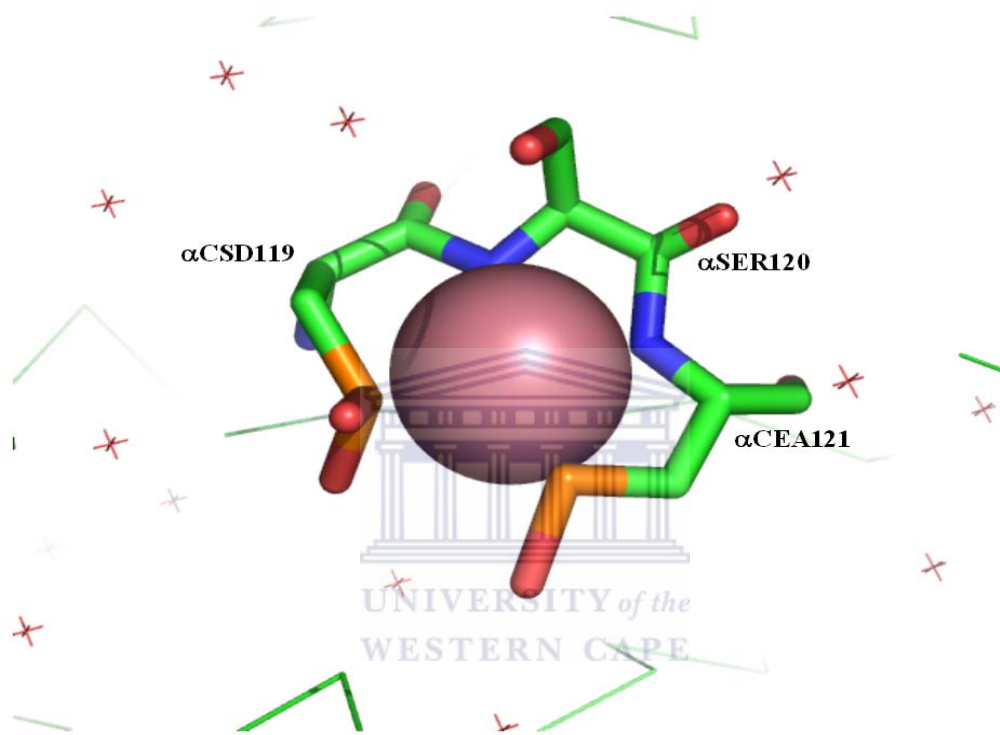


Figure 1.4.3: Cobalt-binding site of NHase showing claw-setting motif. The α CSD119 and α CEA121 represent a sulphenic and sulphonic acids respectively (Tsekoo, 2005).

1.5 *G. pallidus* RAPc8 NHase RAPc8 operon

The *G. pallidus* RAPc8 NHase operon is 5.9 kb long containing eight open reading frames (ORFs) with similar polarity. These are shown in Figure 1.5.1 in order of expression. Amidase is expressed first, followed by the NHase β and α subunits, a 122-amino acid accessory protein (P14K), a homologue of the 2Fe-2S class of ferredoxins and

three putative proteins with distinct homology to the cobalt uptake proteins *cbiM*, *cbiN* and *cbiQ* of the *S. typhimurium* LT2 cobalamin biosynthesis pathway. Each ORF has an ATG start codon and, with the exceptions of NHase α (TAG) and *cbiQ* (TGA), and the TAA termination codon (Cameron *et al.*, 2005)

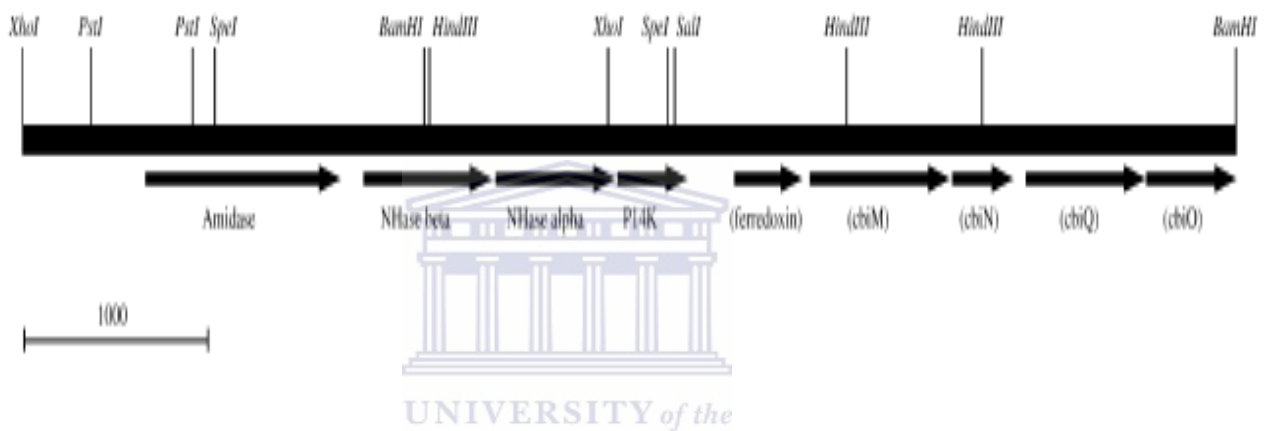


Figure 1.5.1: *G. pallidus* RAPc8 NHase gene cluster showing open reading frames
1 bar = 1000 nucleotides (Cameron *et al.*, 2005)

The NHase genes are located 127 bp downstream of the amidase stop codon. The NHase β subunit gene encodes a 229 amino acid (26.5 kDa) protein, while the NHase α subunit gene encodes a 216 amino acid (24.6 kDa) (Cameron *et al.*, 2005). NHase α contains the CTLCSCY (residues 116–121) cobalt-binding enzyme motif.

With the exception of *Rhodococcus rhodochrous* J1, all known NHases are co-expressed with an amidase (Cameron *et al.*, 2005). The amidase converts the amide product of

NHase to a carboxylic acid with the release of ammonia (Cramp and Cowan, 1999). The amidase is 348 amino acids with a molecular weight of 38.6 kDa (Agarkar *et al.*, 2006). Sequence comparisons suggest that this amidase is a member of the nitrilase superfamily with the glutamate-lysine-cysteine (E-K-C) catalytic triad residues being conserved (Agarkar *et al.*, 2006).

Genes of activator proteins (*p14k*) flank those of the NHase. These activator proteins have been implicated in the expression of functional NHase. An exception is the *Bacillus sp* BR449 NHase, which had no detectable P12K protein expression in *E. coli* (Cameron *et al.*, 2005). The 47 kDa activator protein for Fe-type NHases shares homology with the ATP-dependent iron transporter Mag A, while the 14 kDa activator protein for Co-type NHases shares homology with the NHase β subunit (Cameron *et al.*, 2005).

Heterodimer assembly is believed to be a dynamic process involving the P14K protein, as opposed to it being a passive docking process (Tsekoa, 2005). P14K functions as a subunit-specific chaperone, aiding in NHase α subunit folding prior to α - β subunit association and the $\alpha_2\beta_2$ holoenzyme formation (Cameron *et al.*, 2005). Interaction between the subunits is loose, being formed by amino acids of the β subunit of each dimer.

The heterologous expression mechanism used for *G. pallidus* RAPc8 NHase is facilitated by a host-vector system that was developed in *R. rhodochrous* strains (Cameron *et al.*,

2005). The NHase is recombinantly expressed in *E. coli* BL21 (DE3) pLysS supplied by stratagene (Cameron *et al.*, 2005, Tsekoa *et al.*, 2005).

1.6 Enzyme redesign

The aim of enzyme redesign is to alter enzyme structure to induce a predicted change in function (Penning and Jez, 2001). Some of the techniques applied for enzyme redesign involve chimera formation by site-based domain swap or peptide ligation. Other techniques involve random mutagenesis, which is useful when no structural information is available (Penning and Jez, 2001). Site-directed mutagenesis is a powerful technique commonly used to introduce point mutations. Mutational changes may see alterations in substrate specificity, co-factor requirements, reaction stereochemistry or engineering new catalytic activities (Cedrone *et al.*, 2000).

Comparative analysis of homologous proteins that differ in substrate specificity can influence rational design in an enzyme family (Harris and Craik, 1998). The NHase activity after the substitution Q19E in a cysteine protease increased the turnover number by approximately 10^4 relative to that of the wild-type enzyme. A comparable substitution performed in a mechanistically, but not structurally, related enzyme, asparagine synthetase B (N74D) yielded an increase in activity with a ratio of only 200 between the wild-type and the variant (Cedrone *et al.*, 2000). Figure 1.6.1 shows the different approaches that can be taken to redesign an enzyme.

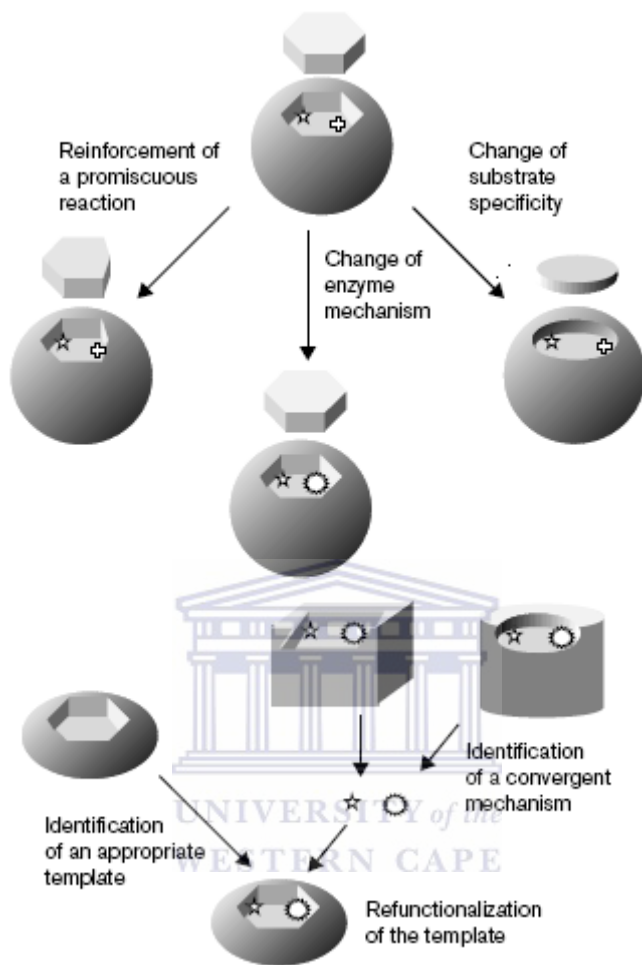
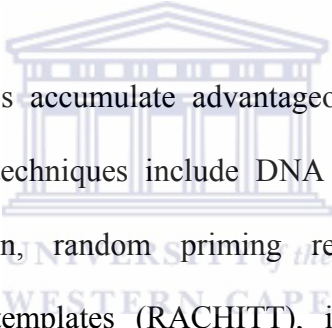


Figure 1.6.1: Four strategies for redesigning enzyme functions (Cedrone *et al.*, 2000)
 The upper part of the figure shows three possible routes to modify a pre-existing enzyme activity into an original one. The fourth strategy is based on the assembling of independent enzyme features to create a novel biocatalyst. The white cross and star depict functional amino acid residues.

Directed evolution is carried out using random mutagenesis or gene recombination techniques to generate genetic diversity (Woodyer *et al.*, 2004). The generated gene library would then be inserted into a well characterised microbial strain for protein expression, followed by the determination of protein functionality, and selection of mutants possessing desirable traits (Woodyer *et al.*, 2004). Random mutagenesis can be

carried out with the use of mutagens, ultraviolet radiation, mutator strains or error-prone (EP-) PCR (Woodyer *et al.*, 2004). EP-PCR involves the use of a low fidelity polymerase such as *Thermus aquaticus* (Taq) polymerase, in combination with unequal nucleotide concentrations and varying Mg^{2+} or Mn^{2+} concentrations. Region-specific random mutagenesis is the preferred method for substrate specificity modulation when the target enzyme has not yet been well characterised. However, although detailed knowledge of the catalytic mechanism and substrate specificity are unnecessary for completely random mutagenesis, success depends on large library searches of the variant proteins in order to identify the desired function (Harris and Craik, 1998).



Gene recombination techniques accumulate advantageous mutations whilst removing deleterious mutations. These techniques include DNA shuffling, staggered extension process (StEP) recombination, random priming recombination (RPR), random chimeragenesis on transient templates (RACHITT), incremental truncation for the creation of hybrid enzymes (ITCHY), and sequence homology-independent protein recombination (SHIPREC) (Woodyer *et al.*, 2004). The process of DNA shuffling involves reiterative mutation and recombination by non-specific DNA fragmentation. This is followed by reassembly and extension of the fragments by primer-less PCR (Harris and Craik, 1998). DNA shuffling is the most commonly used gene recombination technique. In some cases, mutations in areas distant from the active site may influence characteristics such as specificity or stability, as was noted by Stemmer and company in their attempt to direct β -D-fucosyl hydrolysis activity onto β -galactosidase (Harris and Craik, 1998).

1.7 The reaction mechanism of NHases

No consensus has been reached pertaining to the reaction mechanism of NHases, though several models have been proposed. The mechanism proposed by Mitra and Holz (2006) implicated the role of a catalytic triad (Y-W-S) as described in Figure 1.7.1.

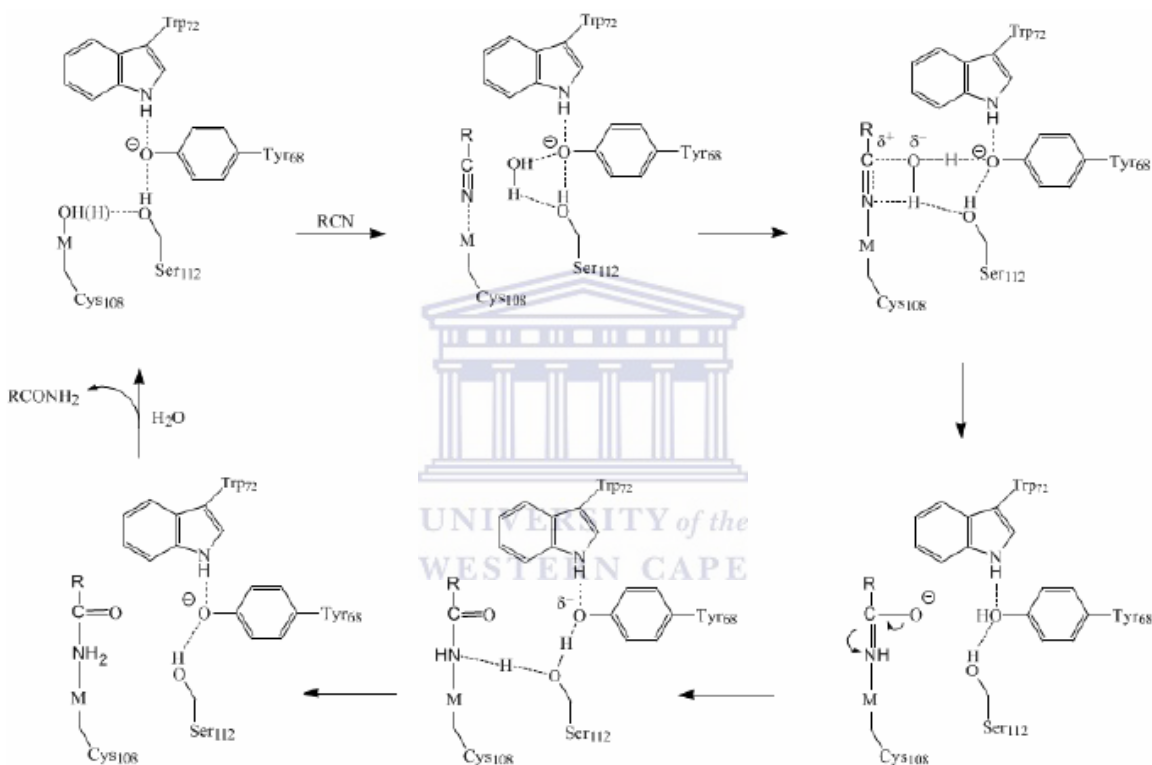


Figure 1.7.1: Tyrosinate base reaction mechanism of NHase (Mitra and Holz, 2006)

The hydrogen that bonds to the indole nitrogen of W76 forms a hydrogen bond with the nucleophilic phenol oxygen of tyrosine 72 (Y72). The phenolic oxygen also forms a hydrogen bond with the side-chain hydroxide hydrogen of S120. The hydroxide oxygen of S120 in turn interacts with one of the hydrogen atoms in a water molecule. The water molecule interacts with the Co ion through the oxygen. The nitrile nitrogen displaces the Co ion coordination complex water molecule, which in turn generates a partially positive

charge in the cyanide carbon through interaction with the electron-rich oxygen. The free water molecule hydrogen forms a bond with the cyanide nitrogen. The water molecule donates a proton to the electronegative tyrosine oxygen and the cyanide nitrogen, while the negatively charged water molecule oxygen bonds to the cyanide carbon, leaving a double bond between the carbon and nitrogen. The negative charge influences the nitrogen to be a nucleophile, causing it to accept the serine residue side-chain proton.

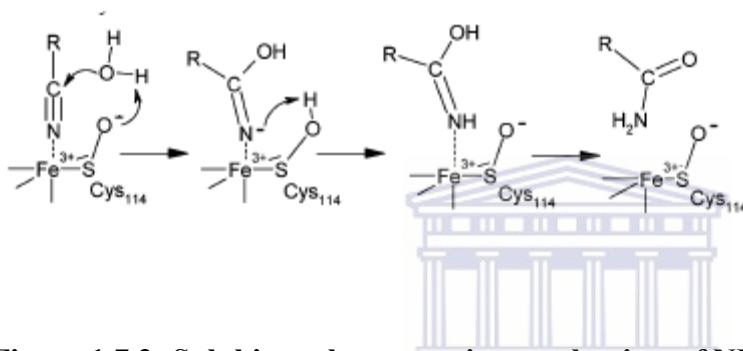


Figure 1.7.2: Sulphinate base reaction mechanism of NHase (Hopmann *et al.*, 2007)

Another proposed mechanism (Hopmann *et al.*, 2007) accounts for the post-translational Sulphur-oxygenation and the roles of the Cys–SOH or Cys–SO₂H ligands in the catalytic activity as shown in Figure 1.7.2. The sulphinate base extracts a proton from the water molecule, forming an OH. This free hydroxide attacks the cyanide carbon, causing it to be electropositive. This in turn generates an electron-rich nitrogen which extracts the sulphinate proton.

1.8 Rationale

Previous work on *G. pallidus* RAPc8 NHase focused on broadening the substrate specificity spectra to include aromatic nitriles. This was based on a postulated hypothesis (Cameron, 2002) suggesting that the lack of aromatic specificity in *G. pallidus* RAPc8 NHase was due to hydrophobic interactions between active site residues and the aromatic substrate, trapping it in a non-catalytic orientation. This may also explain why benzonitrile is a potent inhibitor of the NHase. The pNH14k plasmid was used as the mutagenesis template in which five single mutations were generated; β F36L, β F52G, β F55L, β Y67A, and β W76G (Tsekoo, 2005). Table 1.8.1 gives a comparison of the kinetic constants of inhibition of wild type and β W76G NHase activity on acrylonitrile by benzonitrile.

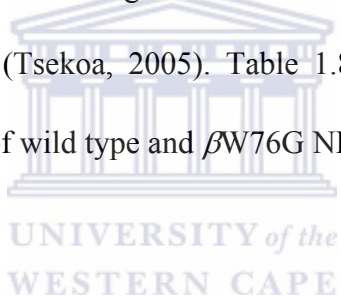


Table 1.8.1: Kinetic constants of wild-type and the β W76G mutated NHase. Acrylonitrile was the substrate in the presence of benzonitrile as the inhibitor as calculated using the direct linear plot (Tsekoo, 2005)

Benzonitrile (μ M)	Wild-type		β W76G	
	K_m (mM)	V_{max} (U/mg)	K_m (mM)	V_{max} (U/mg)
0	10.1	1832	3.87	2011
200	5.29	1016	2.49	1402

Detailed enzymatic assays performed on wild type and the $\beta W76G$ showed no detectable benzonitrile activity, although reduced inhibition of acrylonitrile hydration by benzonitrile was noted. Structural changes noted included an 11 % increase in protein volume and a 20 % decrease in inner surface area of the substrate channel. It was suggested that further amino acid targets for mutation to be located in pocket 55 regions of the substrate channel as the pocket 55 end of the channel is blocked by the N-terminal arm of the cognate dimer (Tsekoa, 2005).

A double mutation; $\beta F52G$ and $\beta F55L$ was introduced into the wild type (Kowlessur *et al.*, unpublished) which showed intrinsic flexibility (Kowlessur *et al.*, unpublished). A flip-flop substrate entry mechanism was proposed for active site function, with the $\beta F52G\beta F55L$ mutant showing activity with benzonitrile. The active site pockets had a 26 % increase in protein volume and a 28 % increase in substrate channel surface area. It was proposed that these changes were associated with aromatic substrate recognition.

Table 1.8.2 shows the effect of a double mutation of two NHase active site aromatic residues on the enzyme's kinetic parameters. The kinetic parameters of wild type NHase are not shown as the enzyme does not hydrate benzonitrile. The *G. pallidus* RAPc8 NHase operates at an optimum pH of 7.0, with a 50 % catalytic activity at pH 5.1 and pH 8.7 (Pereira *et al.*, 1998). Modification of the active site residues are shown to have an effect on substrate specificity.

Table 1.8.2: Kinetic values for *G. pallidus* RAPc8 NHase strains (Kowlessur *et al.*, unpublished)

NHase strain	Nitrile	K_M (mM)	V_{max} (U/mg)	k_{cat} (s^{-1})	k_{cat} / K_M ($mM^{-1}s^{-1}$)
$\beta F55L/\beta F52G$	Benzonitrile	0.31	1100	1800	5900
	Acrylonitrile	2.58	730	1200	450
Wild type	Acrylonitrile	11.50	1300	2100	180

The goal of this work is to gain insight into the catalytic function of NHases, with the long term aim of developing a NHase mutant that has enhanced performance in industrial biotransformation in the process. This study uses site-directed mutagenesis as the method of choice in the catalytic modification of *G. pallidus* RAPc8 NHase, with the generation of the site mutations $\beta Y72F$ and $\beta W76V$ in the *G. pallidus* RAPc8 NHase. The objective was to characterise the kinetic parameters of the *G. pallidus* RAPc8 NHase mutant, comparing them to what is currently known about the wild type. The determinations of the effect of changes in environmental conditions would also be done. Though detailed characterisation of the *G. pallidus* RAPc8 NHase wild type is yet to be completed, the work carried out on *P. thermophila* (Mitra and Holz, 2006) and *Comamonas testosteroni* (Rao and Holz, 2008) NHases would provide a comparative model of the catalytic behaviour of NHases. This would provide information pertaining to the relevance of $\beta Y72$ and $\beta W76$ in the catalytic function of NHases as well as determine whether the sulphinate or the tyrosinate base is responsible for nitrile hydration by NHases.

Chapter 2: Methodology

Chemicals and reagents were supplied by Merck Chemicals and Laboratory Supplies and Sigma-Aldrich Chemical Company. Culture media was supplied by Oxoid Ltd and Biolabs. DNA and protein molecular weight markers, and restriction enzymes were purchased from Fermentas Life Sciences Ltd. Table 2.1 describes the compositions of routinely utilised buffers and solutions.


Table 2.1 Composition of buffers and solutions

Buffer/Solution	Composition	pH
Agarose gel loading dye (6X)	0.25 % (w/v) bromophenol blue 40 % (w/v) sucrose	N/A
1 M Potassium phosphate buffer	717 ml 1 M K ₂ HPO ₄ 283 ml 1 M KH ₂ PO ₄	7.2
SDS-PAGE electrode buffer (10X)	0.25 M Tris-HCl 2 M glycine 1 % (w/v) SDS	8.3
SDS-PAGE Gel-loading Buffer (2X)	100 mM Tris-HCl 4 % (w/v) SDS 0.2 % (w/v) bromophenol blue 20 % (v/v) glycerol 200 mM dithiothreitol	6.8
PAGE staining solution	0.2 % (w/v) Coomassie Blue R 250 40 % (v/v) methanol 10 % (v/v) acetic acid	
PAGE destaining solution	40 % (v/v) methanol 10 % (v/v) acetic acid	
20X TAE buffer	2 M Tris base 25 mM EDTA (pH adjusted with glacial acetic acid)	8.3

2.1 *In silico* procedures

The molecular model generated from the crystal structure of *G. pallidus* RAPc8 NHase (2DPP) was downloaded in PDB format from www.rcsb.org/pdb. The structure was modified with respect to the desired mutations using pyMOL (www.pymol.org). The gene sequence for *G. pallidus* RAPc8 NHase was downloaded from the National Center for Biotechnology Information (NCBI) website (www.ncbi.nlm.nih.gov/). The primers bearing the desired mutations were then designed using the open source online software primer 3 (fokker.wi.mit.edu/primer3/input.htm) and a reverse complement converter (www.bioinformatics.org/SMS/rev_comp.html). The annealing temperatures were determined using the Tm calculator (www.finnzymes.com).

The designed primers were:



Forward β W76V 5' TCGTATTATGGCCATGTGAT 3'

Forward β W76V β Y72F 5' TCGTTCTATGGCCATGTGAT 3'

Reverse β W76 5' ACGACGTCAAATAATCCAAT 3'

The forward and reverse β W76V primers both had a GC content of 40 % whereas the Forward β W76V β Y72F has a GC content of 45 %. All of the primers were found to fulfil the criteria set by the Phusion kit. All primers were HPLC purified and 5' phosphorylated to prevent the formation of smaller PCR products lacking nucleotides at the ligation site. The annealing temperatures were calculated using the Tm calculator (www.finnzymes.com) and were found to operate at temperatures at or above 60°C, the

minimum operating temperatures of the high fidelity Phusion Hot start DNA polymerase.

The primers overlapped by one nucleotide as is required by the Phusion mutagenesis kit.

The DNA sequence of the wild type β subunit is shown in Figure 2.1 below.

```

1      ATGAACGGTATTCATGATGTTGGAGGCATGGATGGATTTGGAAAAGTTATGTATGTAAAA
1      M N G I H D V G G M D G F G K V M Y V K

61     GAAGAAGAGGACATTTATTTTACACATGATTGGGAAAGACTTGCCTTCGGACTTGTAGCT
21     E E E D I Y F T H D W E R L A F G L V A

121    GTTTGTATGGCACAAGGATTGGGGATGAAGGCTTTTGTATGAATTCAGGATCGGCATTGAG
41     G C M A Q G L G M K A F D E F R I G I E

181    CTTATGCGTCCAGTGGATTATTTGACGTCGTCGTATTATGGCCATTGGATTGCAACCGTT
61     L M R P V D Y L T S S Y Y G H W I A T V

241    GCATACAACCTTAGTAGATACGGGAGTATTAGACGAAAAAGAACTAGATGAACGAACGGAG
81     A Y N L V D T G V L D E K E L D E R T E

301    GTTTTCTTGAAGAAACCTGATACCAAAATACCACGAAGAGAGGATCCGGCATTAGTGAAG
101    V F L K K P D T K I P R R E D P A L V K

361    CTTGTAGAAAAGGCACCTGTATGATGGCTTATCTCCGCTCCGTGAAATTTTCAGCTTCTCCT
121    L V E K A L Y D G L S P L R E I S A S P

421    CGGTTTAAGGTAGGAGAGAGAATCAAGACGAAAAACATTCATCCAACCTGGTCATACGAGA
141    R F K V G E R I K T K N I H P T G H T R

481    TTCCCTCGATATGCCCGTGACAAATATGGTGTTCATTGATGAGGTATATGGAGCTCATGTT
161    F P R Y A R D K Y G V I D E V Y G A H V

541    TTCCCTGATGATGCTGCTCATAGAAAAGGAGAAAACCCGCAATATCTTTACCGGGTACGT
181    F P D D A A H R K G E N P Q Y L Y R V R

601    TTTGAGGCTGAAGAATTATGGGGATATAAACAGAAAGATTCCGTTTATATAGATCTATGG
201    F E A E E L W G Y K Q K D S V Y I D L W

661    GAAAGTTATATGGAGCCTGTTTCACATTAA
221    E S Y M E P V S H *

```

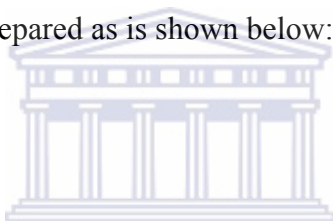
Figure 3.3.1: DNA and amino acid sequences of the *G. pallidus* RAPc8 NHase β subunit.

There is one stop codon which is positioned right at the end of the sequence. This makes the largest open reading frame 687 bp long, generating 229 amino acids and a protein that is 26 477 Da in size. The region highlighted in grey and underlined represent the forward and reverse primers, respectively. The letters in bold represent the amino acids targeted for substitution. In the forward primer, TAT was to be replaced by TTC, while TGG was to be replaced by GTG.

2.2 Site-directed mutagenesis

The mutagenesis primers were synthesised by Integrated DNA Technologies (IDT) Inc. They were HPLC purified and 5' phosphorylated. The Phusion Site directed mutagenesis kit used was supplied by Finnzymes. The plasmids used in this work were pET21a(+) derivatives. They were pNH14K (also referred to as pNH461), which carries the NHase α and β subunit genes as well as the P14K gene of *Geobacillus* sp.RAPc8. (Cameron *et al.*, 2005), pNH14K F52G, carrying the NHase and pNH14K F55L, carrying the NHase F55L mutant of pNH14K (Tsekoa, 2005). The mutagenesis was carried out by PCR.

The reaction master mix was prepared as is shown below:

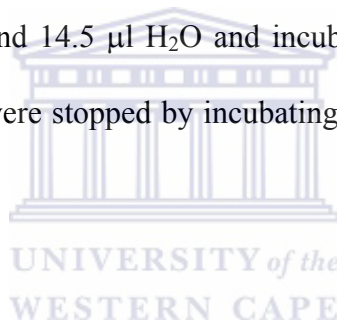


Component	Volume / 50 μ l reaction	Final concentration
5x Phusion HF Buffer	10 μ l	1x
10 mM dNTPs	5 μ l	1000 μ M each
Forward primer	0.5 μ l	0.125 μ M
Reverse primer	0.5 μ l	0.125 μ M
Template DNA	1 μ l	
Phusion Hot Start DNA Polymerase	0.5 μ l	0.02 U/ μ l
H ₂ O	32.5 μ l	

The cycle parameters were as follows:

Cycle step	Temperature	Time	Number of cycles
Initial denaturation	98°C	30 s	1
Denaturation	98°C	5-10 s	
Annealing	65-72°C	10-30 s	25
Extension	72°C	5 min	
Final extension	72°C	5-10 min	1
Hold	4°C		

After the reaction, the PCR products were separated on a 1 % agarose gel with 10 mg/ml ethidium bromide. One μ l of each of the PCR products was added to 0.5 μ l T4 DNA ligase, 4.0 μ l ligation buffer and 14.5 μ l H₂O and incubated at room temperature for 2 hours. The ligation reactions were stopped by incubating the ligation mixtures in a 65°C water bath for 15 minutes.



2.3 Preparation and transformation of electrocompetent cells

The *E. coli* strains used in this work were BL21 (DE3) pLysS, an expression vector supplied by Stratagene, and Genehog, a cloning vector supplied by Invitrogen. The BL21 (DE3) *E. coli* strain possessed the genotype *hsdS gal ompT (cIts857 ind1 Sam7 nin5 lacUV5-T7 gene1)*, whereas the Genehog possessed the genotype F- *mcrA D(mrr-hsdRMS-mrcBC) f80lacZDM15 DlacX74 deoR recA1 endA1 araD139 D(ara-leu)7697 galU galK l rpsL nupG* .

Glycerol stocks of the two bacterial strains were streaked on LB agar plates and grown at 37°C overnight. This was followed by the preparation, inoculation and orbital incubation of 5 ml LB vials.

The vials were used to inoculate 400 ml of SOC media in 2 L conical flasks to a ratio of 1: 200. The SOC media was incubated at 37°C until an OD_{600nm} of 0.6 was reached. The cells were harvested, followed by a ddH₂O wash and centrifugation. An additional wash using 10 % glycerol, followed by one using 15 % glycerol and 2 % sorbitol was performed. All centrifugations were done at 4000 x g for 10 min. The cells were then diluted with 15 % glycerol and 2 % sorbitol to an OD_{600nm} of 200-250. Fifty ml aliquots were placed in eppendorf tubes, which were immersed in absolute ethanol at -80 °C. The cells were then stored at -80 °C until they were ready for use.

Electroporation was carried out using the Biorad Gene Pulser™. The resistance, capacitance and voltage were set at 200 Ω, 25 μF and 1.8 kV, respectively. Pre-chilled cuvettes with 0.1 cm gaps were used. One μl of the ligated DNA mixture was added to 50μl of Genehog electrocompetent cells on ice. After a gentle mix, the cells were transferred to a cuvette in a way that ensured the absence of air bubbles. Immediately after electroporation, 1 ml of SOB was added to the cuvette. The cuvette contents were then transferred to 2 ml eppendorf tubes for a 45 min recovery at 37°C. The cells were then plated onto selective LB media with 100 μg/ml ampicillin and grown overnight at 37°C.

2.5 Verification of transformation and mutagenesis success

After 16–20 hours, five colonies were selected from each plate. Plasmid extraction was carried using the Invisorb™ spin Plasmid mini two (250) kit (Invitek). The only modification of the method involved the use of 10 mM Tris pH 8 as opposed to the elution buffer provided. A PCR reaction was carried out on the plasmids using T7 primers, the sequences of which are listed below:

T7promoter TAATACGACTCACTATAGGG

T7terminator GCTAGTTATTGCTCAGCGG

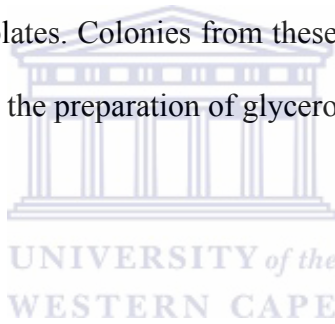


The following cycling parameters were used for this step:

Cycle step	Temperature	Time	Number of cycles
Initial denaturation	94°C	30 s	1
Denaturation	94°C	5-10 s	
Annealing	52°C	10-30 s	25
Extension	72°C	15-30 s /1 kb	
Final extension	72°C	5-10 min	1
Hold	4°C		

After the reaction, the PCR products were separated on a 1 % agarose gel with 10 mg/ml ethidium bromide. 10 µl aliquots of the plasmid DNA samples that were amplified by the T7 primers were sent for sequencing at the Molecular Cell Biology Sequencing Unit, University of Cape Town.

Plasmid DNA found to possess the desired mutation was used to transform BL21 DE3 (pLysS) electrocompetant cells. The cells were used to inoculate LB plates containing ampicillin and chloramphenicol. Verification was carried out by performing the T7-PCR described above. Colonies found to possess the plasmid were re-streaked onto fresh LB plates. Colonies from these plates were used to inoculate 5 ml vials of LB, followed by the preparation of glycerol stocks which were stored at -80 °C.

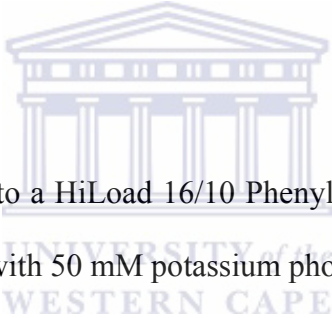


2.6 Expression of the NHase mutants

The glycerol stocks were used to inoculate 5 ml of LB which were grown overnight. The cultures were then used to inoculate 2 L of LB containing 50 µg/ml ampicillin and 30 µg/ml chloramphenicol. The conical flasks were incubated at 37°C and 220 rpm until an OD^{600nm} of 0.4 was reached, when CoCl₂ was added to a final concentration of 0.1 mM. After 15 – 30 min, IPTG was added to a final concentration of 0.4 mM. The cells were harvested and washed with 50 mM potassium phosphate buffer, pH 7.2, about 4 hours after induction.

2.7 Purification of NHase mutants

Washed cell pellets were resuspended in 25 ml of 50 mM potassium phosphate buffer, pH 7.2, followed by a freeze-thaw cycle (-80 to 37°C) and sonication using a Bandelin Sonoplus HD2070 sonicator in cycles of 30 s pulse, 30 s stop for 8 minutes. Centrifugation at 5000 x g for 20 min was carried out and the supernatant was passed through a 0.22 micron filter. $(\text{NH}_4)_2\text{SO}_4$ was added to the supernatant to achieve 20 % saturation. Precipitated proteins were removed by centrifugation at 7000 x g for 30 min at 4 °C.



The supernatant was loaded onto a HiLoad 16/10 Phenyl-Sepharose column (Amersham Biosciences, UK) equilibrated with 50 mM potassium phosphate buffer pH 7.2 containing 1.0 M $(\text{NH}_4)_2\text{SO}_4$. Bound proteins were eluted with a linear gradient of decreasing $(\text{NH}_4)_2\text{SO}_4$ concentration generated with 50mM potassium phosphate buffer, pH 7.2 (5 column-volumes, 1.0M - 0M $(\text{NH}_4)_2\text{SO}_4$). The fractions representative of the peaks observed on the chromatogram were tested for NHase activity using acrylonitrile as a substrate.

Fractions containing NHase were pooled, dialysed against 25 mM potassium phosphate buffer pH 7.2, and loaded onto a HiLoad 26/10 Q-Sepharose column (Amersham Biosciences) equilibrated with the same buffer. Bound proteins were eluted with a linear

gradient of increasing NaCl concentration generated with 25 mM potassium phosphate buffer containing 500mM NaCl (5 column volumes, 0 - 500mM NaCl).

Fractions containing NHase were pooled, dialysed and concentrated. The NHase samples were loaded on a Sephacryl S300 gel filtration chromatography media packed in a XK26/100 column (Amersham Biosciences, UK) equilibrated with 25mM potassium phosphate buffer, pH 7.2 and run at a flow-rate of 0.8 ml min^{-1} for 1.5 column volumes.

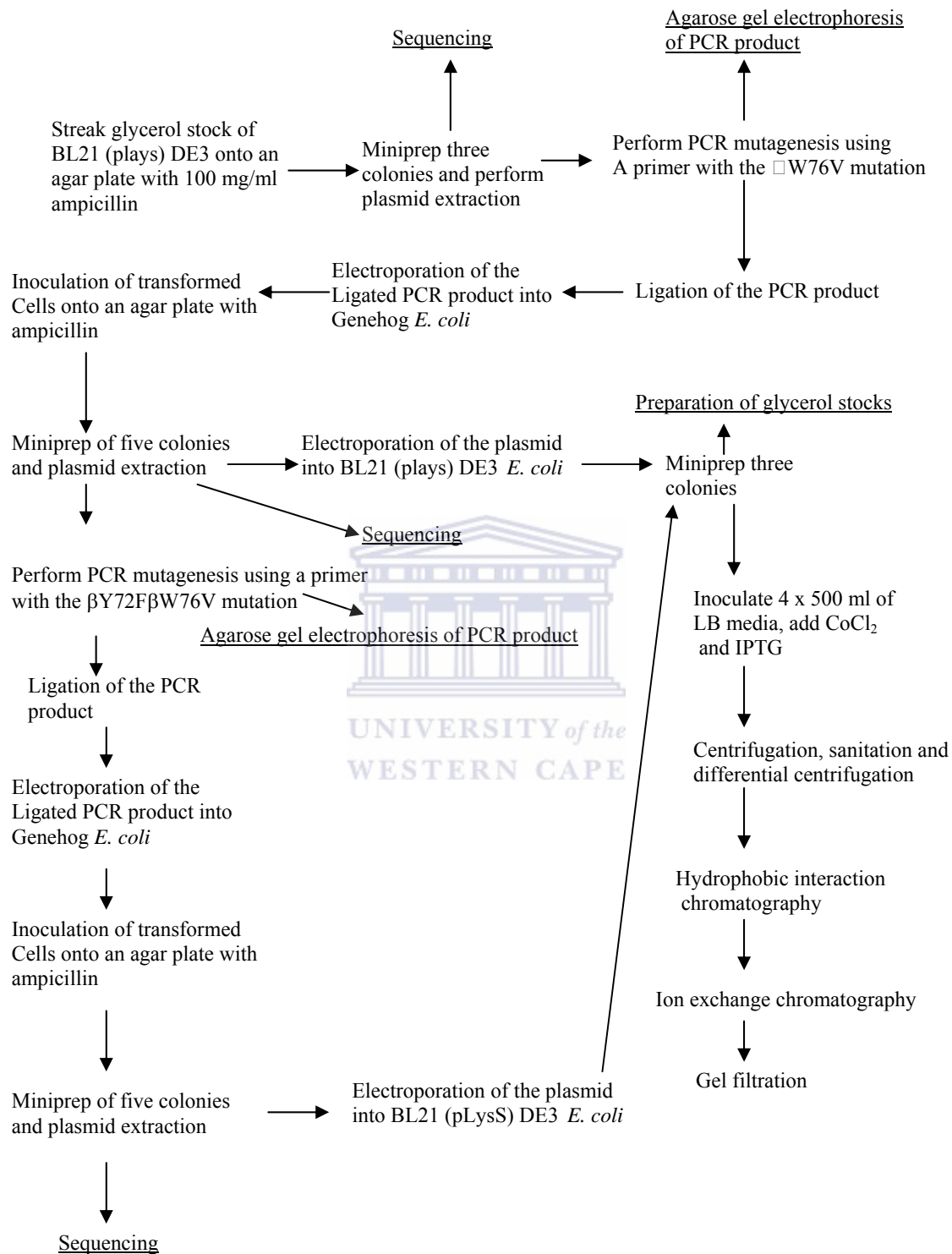
The presence of the functional protein was confirmed using the NHase assay. The molecular weight of the protein was determined using SDS-PAGE (Laemmli *et al.*, 1970), whereas protein concentrations were determined using the modified Bradford assay (Zor and Selinger, 1987) at 595 nm and the direct spectrophotometric assay at 280 nm. The molar extinction coefficient used was $78090 \text{ M}^{-1} \text{ cm}^{-1}$ as determined using the open source PROTPRAM tool (<http://au.expasy.org/tools/protparam.html>).

2.8 Enzyme kinetics

NHase activity was monitored on a Cary 300 Bio spectrophotometer operated via WinUV software (Varian Inc., USA). Reactions were carried out at 50°C in 1 ml quartz cuvettes. All substrates were dissolved in methanol. Prior to the addition of enzyme, the cuvette was incubated at 50°C in order to allow the reaction mixture to equilibrate. Kinetic parameters were determined using acrylonitrile, 3-cyanopyrimidine and benzonitrile as substrates. Acrylonitrile has a boiling point of 77°C and a solubility of $7 \text{ g (100 ml)}^{-1}$ at

20 °C while acrylamide has a solubility of 204 g(100 ml)⁻¹ at 25 °C. The molar extinction coefficients and optimum wavelengths for benzamide and acrylamide are 5.5 and 2.9 mM⁻¹cm⁻¹, and 242 and 225 nm, respectively. The kinetic studies were initially performed to determine the V_{max}, K_m and k_{cat} of the mutant. These kinetic parameters were then determined under different pH and temperatures.





Chapter 3: The engineering, expression and purification of *G. pallidus* RAPc8 NHase

3.1 Introduction

The goal of this work was to determine whether there was a change in NHase activity after the site-directed mutagenesis of conserved residues that have been implicated in the reaction mechanism. This initially involved *in silico* alignment of the two molecular models generated from the crystal structures of *Pseudocardia thermophila* NHase (1IRE) and *G. pallidus* RAPc8 NHase (2DPP) using pyMOL. This software was used to induce site specific mutations in the *in silico* model previously generated from the crystal structure of *G. pallidus* RAPc8 NHase (Tsekoa, 2005). Primers possessing the desired mutations were designed using online Primer 3 tool, taking into account the specifications required by the Phusion kit. The site-directed mutagenesis was carried out following the PCR conditions specified for the Phusion kit.

Agarose gels were run to determine whether or not the PCR reaction had been a success. This was followed by the determination of enzyme activity in the total cell protein of the recombinant strains. Plasmids were extracted from strains showing enzyme activity and sent for sequencing. The plasmid was used to transfected into electrocompetant BL21 (DE3) pLysS *E.coli* cells, which were used to over express the mutated protein. The cells were harvested for subsequent purification of the protein.

3.2 *In silico* procedures

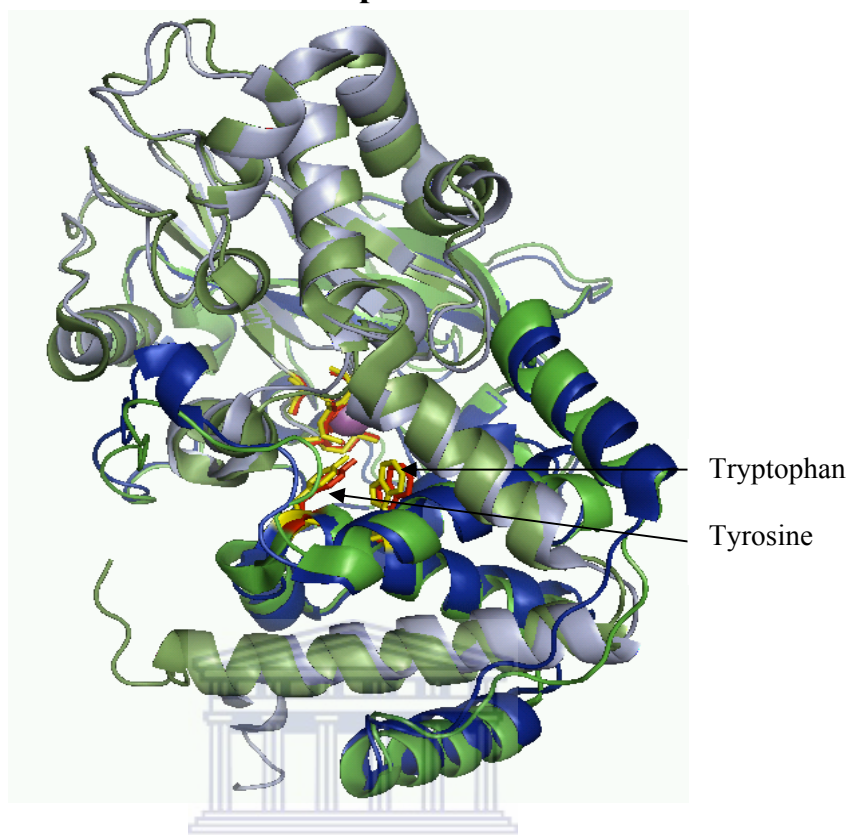


Figure 3.2.1: Alignment of the molecular structures of *G. pallidus* RAPc8 NHase (2dpp) and *P. thermophila* NHase (1IRE)

The ribbon diagram shows the heterodimers of the *P. thermophila* and *G. pallidus* RAPc8 NHase which are shown in blue and green respectively. The α subunits are shown in pale shades, whereas the β subunits are brightly coloured.

The functional conformation of both residues shown in Figure 3.2.1 is the heterotetramer, which consists of two α and two β subunits. The trivalent Co metal ion, shown as a magenta sphere, is surrounded by a “claw setting” coordinate complex of 3 cysteine residues, 2 amide nitrogens and a water molecule. The residues suggested hypothesised to play a role in the reaction mechanism are Y68, W72, C108 and S112 in *P. thermophila* (in yellow) and Y72, W76, C116 and S120 in *G. pallidus* RAPc8 (in red) . The upper arrow shows the W residues, while the lower arrow shows the Y residues for both enzymes. The mutations selected were based on the tyrosinate mechanism, with the

Y72F and W76V chosen as the appropriate substitutions. W76V is a non-conservative, cavity creating mutation that has been selected to determine whether or not W76 plays a role in the NHase mechanism as was previously suggested (Mitra and Holz, 2006).

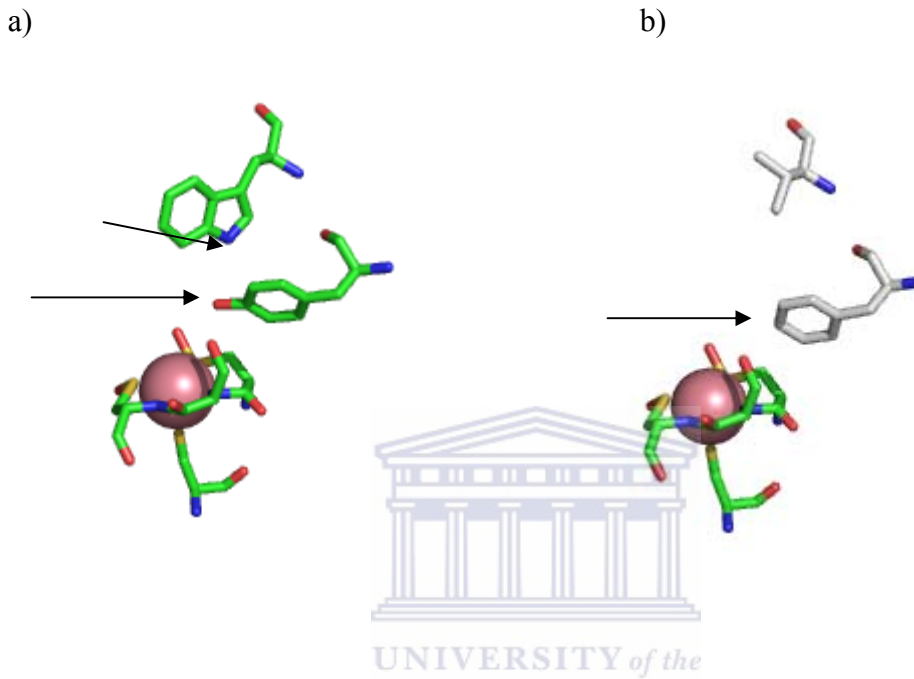


Figure 3.2.2: Active site residues of the *G. pallidus* RAPc8 NHase

The nitrogen, oxygen and sulphur atoms are shown in blue, red and yellow respectively. The wild type and mutated residues can be differentiated by the colour of their carbon atoms, shown in green and grey respectively.

Figure 3.2.2 shows the active site residues (a) before and (b) after mutagenesis. Both active site residue illustrations show the claw setting configuration clustered around a Cobalt ion. A water molecule is the sixth member of the coordinate complex, though it is not shown in the images. The active groups in the substituted residues are shown by the arrows. The Y72F removes the phenolic oxygen, while the W76V mutation removes the indole nitrogen.

3.3 Site directed mutagenesis

The first protocol carried out was the verification of the plasmid possessing the NHase gene. The glycerol stock of the *E. coli* strain possessing the mutated plasmid was used to inoculate 5 ml of media. The inoculated media was incubated overnight at 37°C. Then, the plasmid was extracted and sent for sequencing. The sequence was submitted to ncbi BLAST for identification. The result is showed 99 - 100 % homology with the *Bacillus sp.* RAPc8 NHase sequence.

The plasmid was used for the PCR-based W76V site directed mutation reaction to following the conditions stated in section 2.2 of the Methodology section. The PCR product was ligated and electroporated into Genehog *E. coli*. The *E. coli* was plated and five colonies were selected for 5 ml vial inoculation, cultivation, glycerol stock preparation and plasmid extraction. The plasmid was sequenced and analysed using BioEdit and DNAMAN. No detectable mutation was noted following the use of this primer, with an identical sequence to the wild type being observed. This was an unusual result given that the average efficiency rate for the Phusion site-directed mutagenesis kit is 80 %. The process was successful when repeated using the β W76V β Y72F primer as shown in Figure 3.3.1 below.

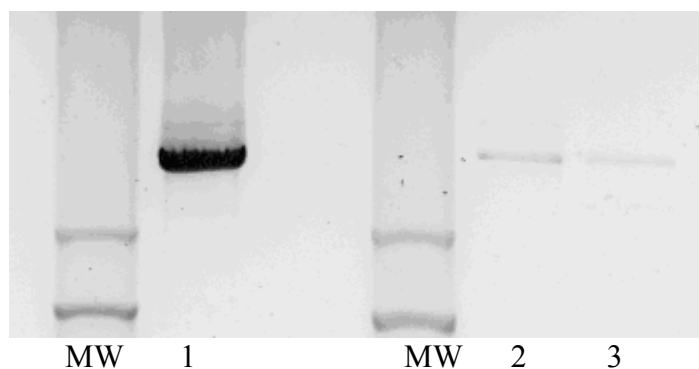


Figure 3.3.1: Agarose gel of the PCR products. MW denotes λ DNA, the molecular weight marker. Lanes 1, 2 and 3 denote the PCR products for the double mutant $\beta Y72F\beta W76V$, and the single mutant $\beta W76V$, together with the linearised wild type respectively.

The PCR products were separated on a 1 % agarose gel with 10 mg/ml ethidium bromide. The wild type was digested prior to gel separation using NdeI restriction enzyme, which is specific for the CATATG restriction site, cutting between the second and third bases (A and T respectively). The $\beta W76V\beta Y72F$ plasmid DNA sequence was aligned with the primer using DNAMAN, which confirmed the presence of a double mutation in the sequence. However, the codon ATC was observed as opposed to TTC, suggests the presence of isoleucine (Y72I) as opposed to Y72F. Considering the large size of the plasmid, and the High fidelity polymerase used for the mutagenesis with a fidelity value of 4.4×10^{-7} , the PCR product would have a 11 % probability of possessing a polymerase induced error. It should be noted that the DNA sequence can not provide a complete picture of the protein structure, as it does not account for post-translational modifications. Two possible techniques that could be used to confirm the structure and amino acid sequence of the functional protein are tandem mass spectrometry and X – ray crystallography.

The $\beta Y72F\beta W76V$ mutant tested positive for NHase activity using the enzyme assay described in section 2.8. It was subsequently expressed, harvested, sonicated and incubated in an ammonium sulphate solution prior to the hydrophobic interaction chromatography.

3.4 Protein purification and expression

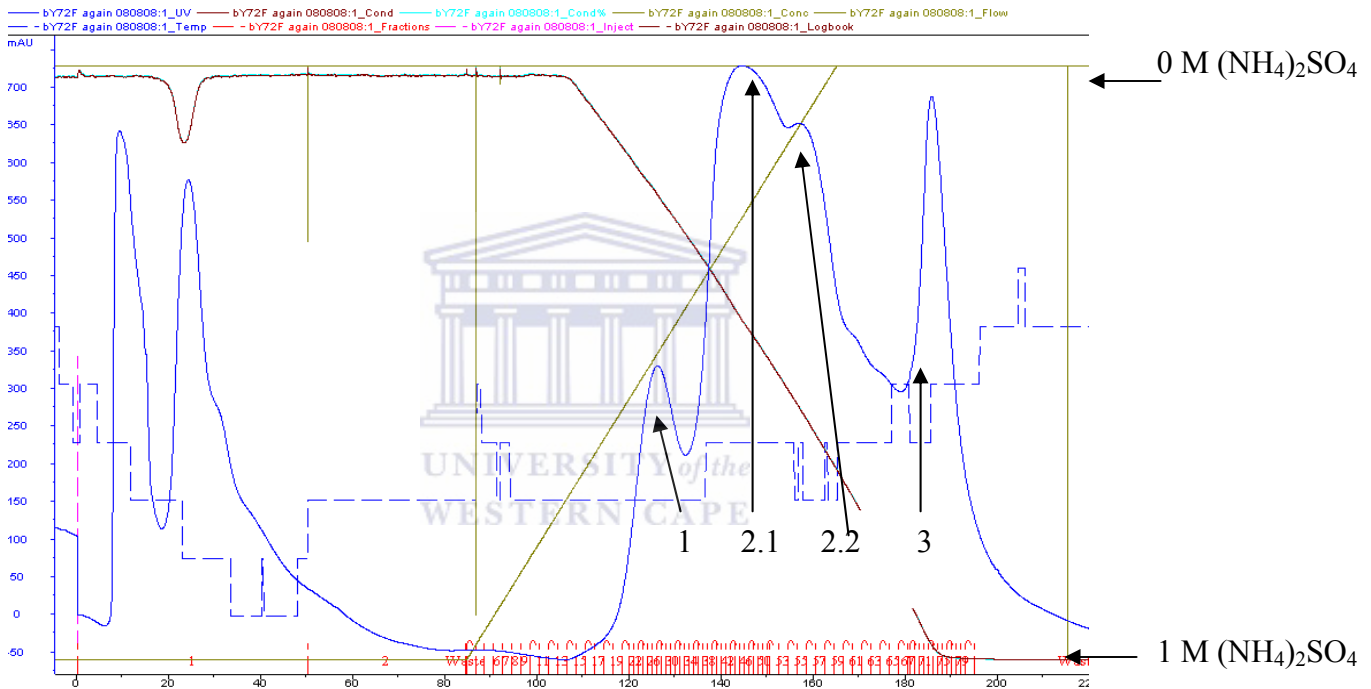


Figure 3.4.1: Hydrophobic interaction chromatogram of the $\beta Y72F\beta W76V$ mutant NHase. The green upward slope is the negative gradient representing the ammonium sulphate concentration from 1 – 0 M, while the purple downward slope represents ion concentration. The wavy blue line denotes the absorbance values of the solution passing through the column. The first two peaks represent the flowthrough, which is the protein that did not bind to the column. The peaks that appear under the upward slope represent the eluted protein fractions. The short vertical lines at the base of the chromatogram represent the 2 ml fractions in which the elute was collected.

The HIC protocol yielded a chromatogram with four peaks; designated peaks 1, 2.1, 2.2 and 3 respectively. The combined peaks could have been avoided and there would have

been a better separation of peaks had the flow rate been reduced (Scopes, 1994). All of the peak aliquots were pooled and tested for activity, with Peak 1 testing positive for the presence of functional enzyme.

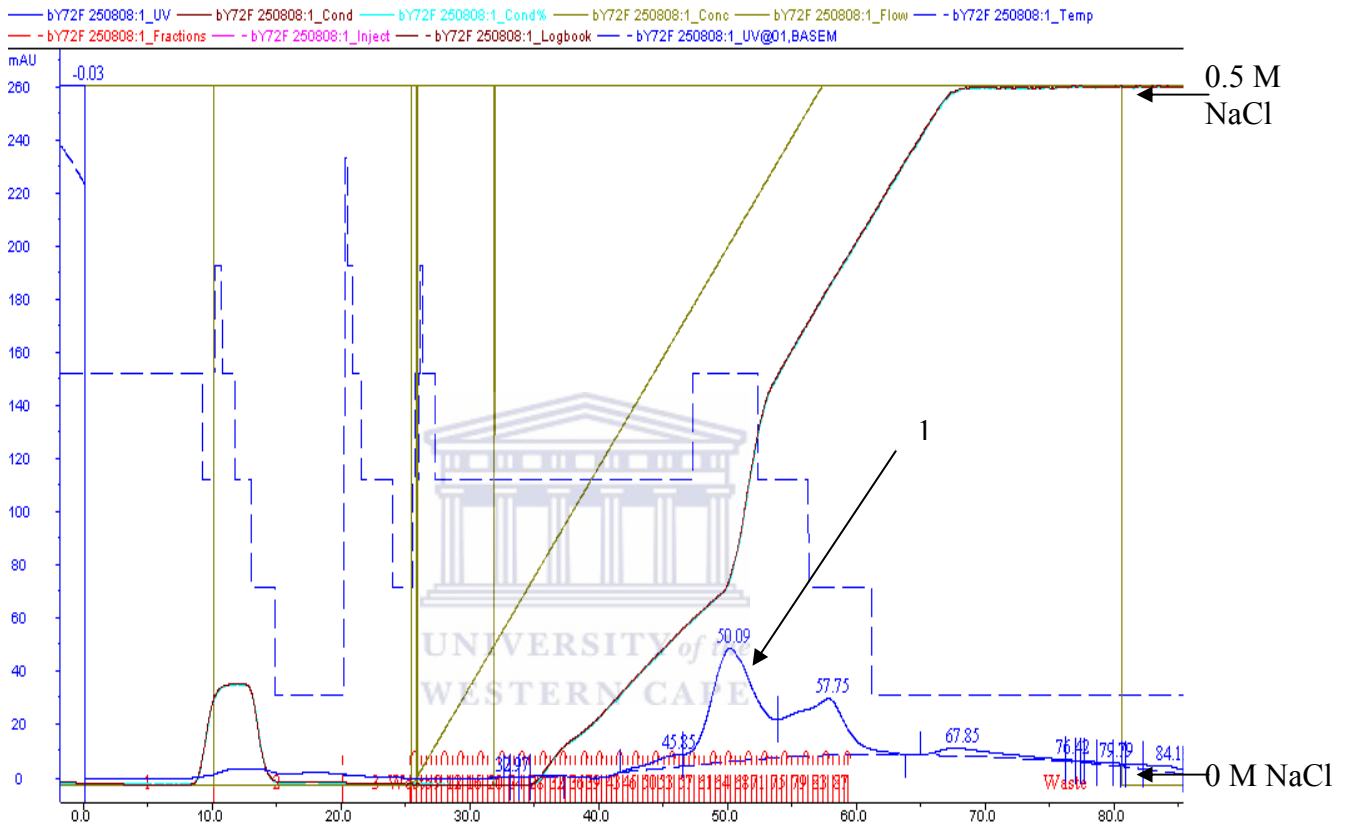


Figure 3.4.2: Ion exchange chromatogram of the $\beta Y72F/\beta W76V$ mutant NHase. The green upward slope is the positive gradient representing the rise in NaCl concentration from 0 – 0.5 M, while the dark purple upward slope represents ion concentration. The wavy blue line denotes the absorbance values of the solution passing through the column. The peaks that appear under the upward slope represent the eluted protein fractions.

The anion exchange chromatogram showed two peaks eluted at sodium chloride concentrations between 150 and 250 mM. The NaCl concentration that resulted in the elution of the two peaks was comparable to the concentration required for the single IEC elution peak of the wild type (Tsekoa, 2005). Enzyme activity was noted in the 150 – 400

mM peak, whereas no such activity was noted in the 400 – 500mM peak. A loss of stability as a result of a high ionic concentration would be expected for most proteins. In addition, the conformation of the mutant may have been disrupted by the occurrence of Donnan effects, which repel protons within the adsorbent to the extent that the matrix pH is up to one unit higher than the buffer (Scopes, 1994).

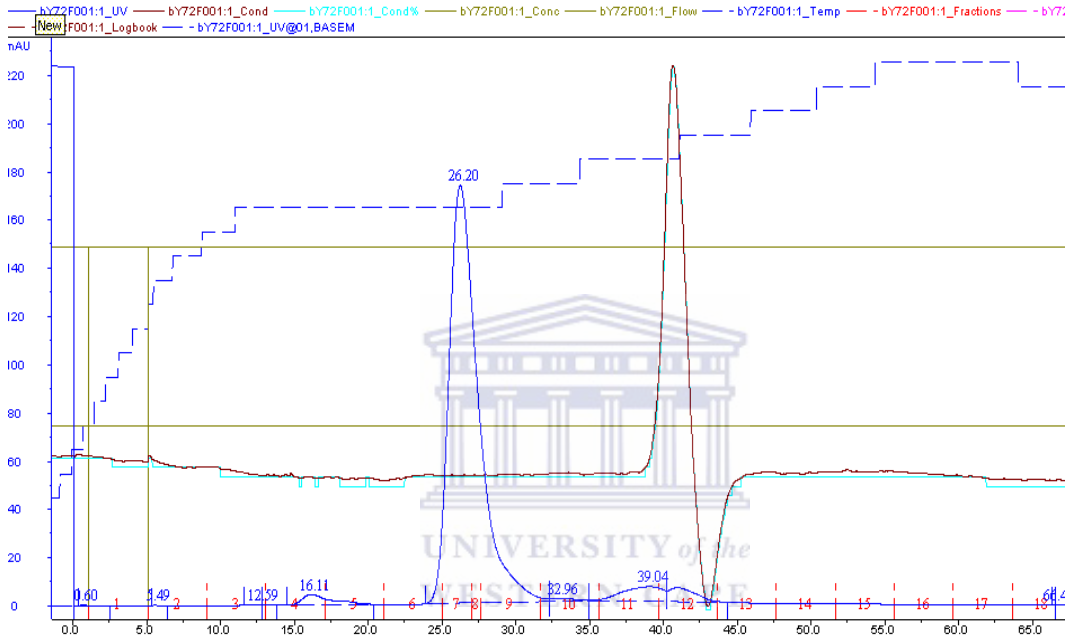


Figure 3.4.3: Gel filtration chromatogram of the $\beta Y72F/\beta W76V$ mutant NHase. The green horizontal line represents the absence of a gradient, as only one buffer solution was used. The wavy blue line denotes the absorbance values of the solution passing through the column. The ion concentration is relatively constant, as shown by the purple line, though one huge fluctuation was briefly noted in elution fraction 12.

The fraction eluted by the ion exchange column was passed through a gel filtration column. The chromatogram is shown above. The single peak detected in the gel filtration chromatogram confirmed the purity and the presence of the enzyme.

The concentrations of all of the purification steps were determined using the modified Bradford assay (Zor and Selinger, 1995) as shown by the standard curve in Figure 3.4.4 and the data in Table 3.4.1.

Figure 3.4.4: Modified Bradford assay standard curve (Zor and Selinger, 1995).

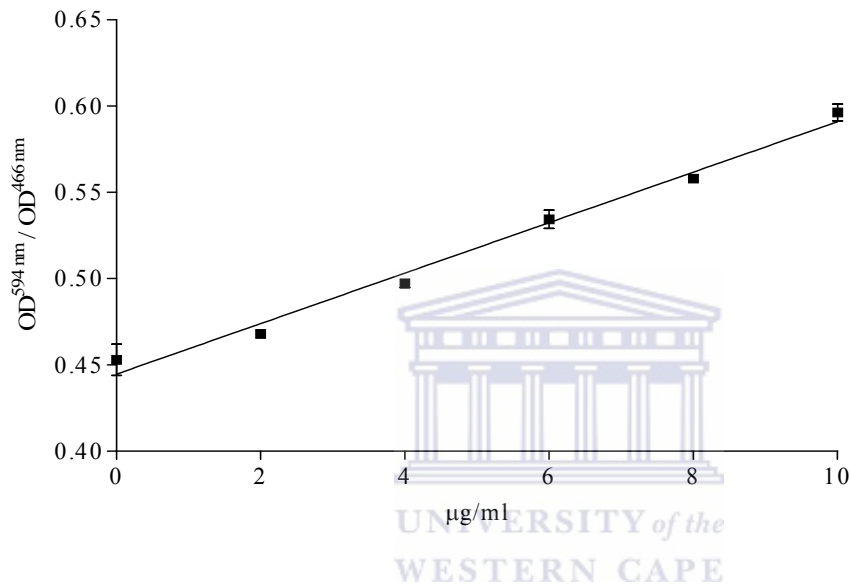


Table 3.4.1: Purification table of the β Y72F β W76V mutant NHase

Step	Volume (ml)	[Protein] (mg/ml)	Total protein (mg)	Specific activity (U/mg)	Total activity (U)	Purification (fold)	Yield (%)
TCP	50.0	4.8	241.0	0.3	72.3	1	100.0
TSCP	45.0	1.2	55.0	0.6	33.0	2	23.0
HIC	17.0	0.1	1.6	1206.0	1929.6	4020	0.7
IEC	14.0	0.1	1.4	656.0	918.4	2186.7	0.6
GF	1.2	2.0×10^{-2}	3.0×10^{-2}	ND	ND	ND	1.0×10^{-2}

The TCP, T SCP, HIC, IEC and GF wells represent the total cell protein, total soluble cell protein, the hydrophobic interaction, ion exchange and gel filtration protein fractions, respectively. The specific activity of the gel filtration is not given because it was not assayed.

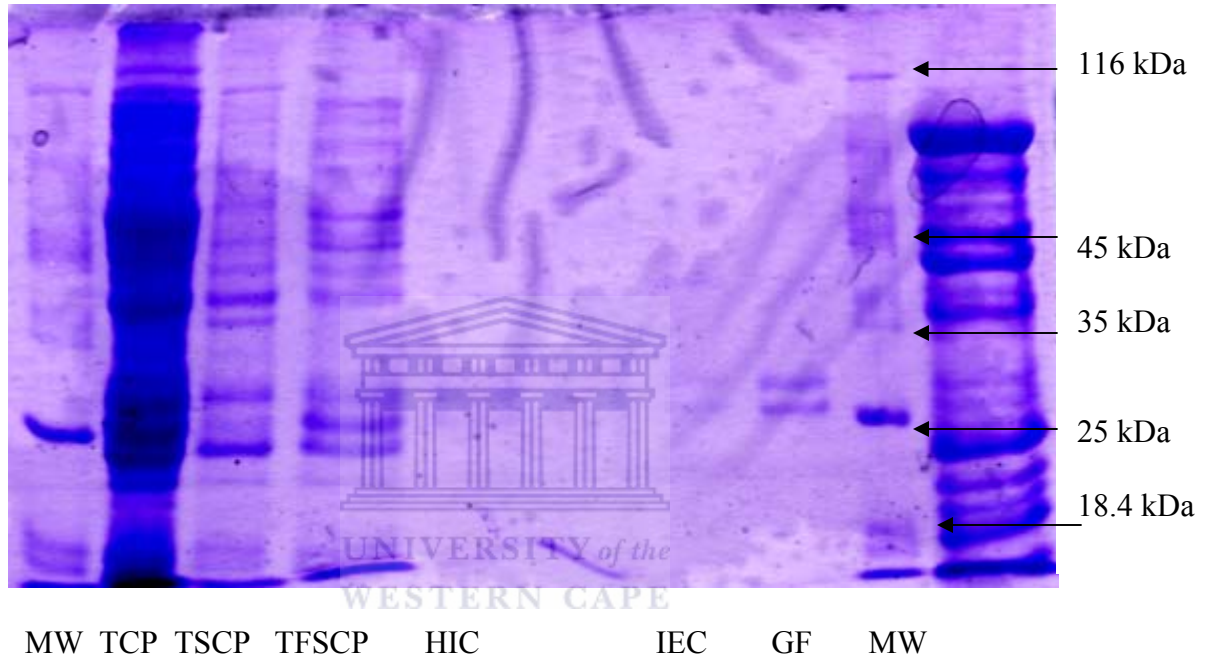


Figure 3.4.5: SDS – PAGE gel of the $\beta Y72F\beta W76V$ protein fractions. The GF, IEC, TFSCP, TSCP, MW and TCP represent the gel filtration, the ion exchange, the hydrophobic interaction, the filtered soluble cell protein, the soluble cell protein, molecular weight and the total cell protein fractions respectively.

The protein concentrations and enzyme activity values were used to generate the purification table (table 3.4.1). A loss in activity was noted in the ion exchange fraction. This may have been as a result of salt concentration which was between 0.3 and 0.4 M. Most enzymes exhibit depressed activity at NaCl concentrations above 0.2 M (Scopes, 1994).

The protein fractions were separated on an SDS-PAGE gel shown in figure 3.4.5. The molecular weight marker used was the Fermentas unstained protein weight marker #SM0431. The standard protein sizes covered by the marker ranged from 14.4 to 116 kDa. Figure 3.4.6 is the graph of the logarithm of molecular weight against the distance travelled on the gel. The $\beta Y72F\beta W76V$ mutant NHase α and β subunits were estimated to be 28.1 and 25.1 kDa, respectively.

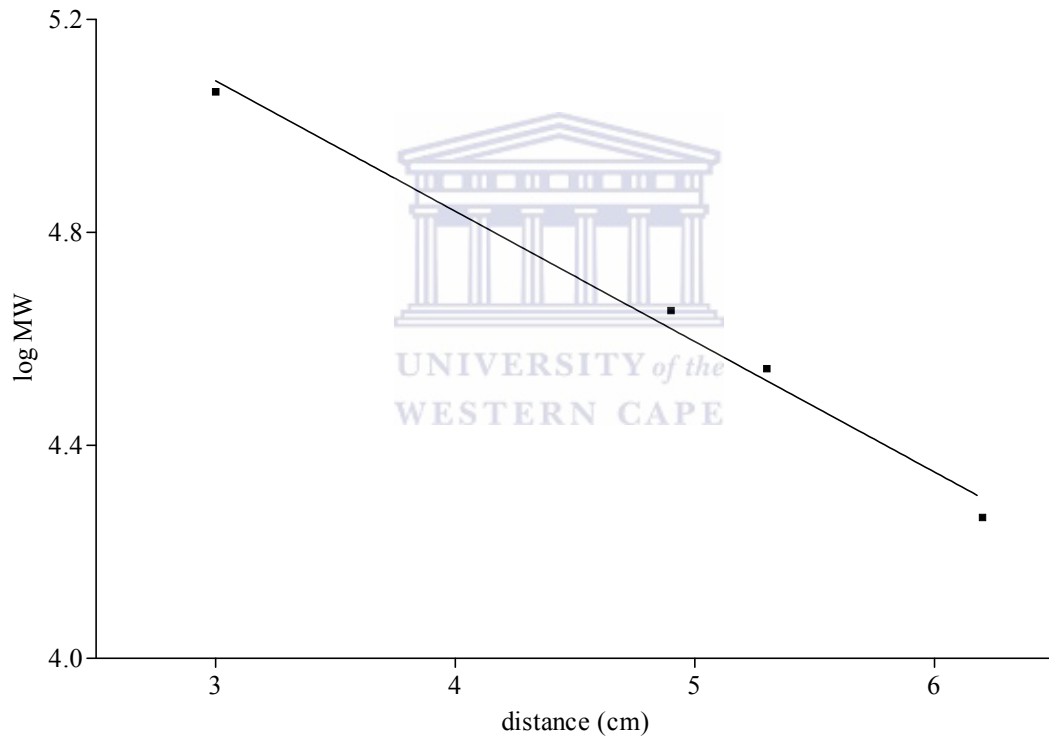


Figure 3.4.6: Standard curve of the logarithm of the molecular weight markers against the distance travelled on the SDS-PAGE gel.

Chapter 4: Kinetic analysis of the $\beta Y72F\beta W76V$ mutant

NHase

4.1 Absorption spectra, calibration and preliminary assays

Figure 4.1.1 shows the absorption spectra of acrylonitrile, acrylamide and 25 % methanol (v/v). The absorption spectra of the amide and nitrile overlap, the absorbance of acrylonitrile is not detectable at wavelengths above 225 nm. Therefore, acrylamide production could be detected between 225 and 270 nm. According to the figure below, the maximum absorbance of acrylamide is at 230 nm. However, the assays were performed at 225 nm in order to ensure comparability with previous work on *G. pallidus* RAPc8 NHase (Tsekoa, 2005).

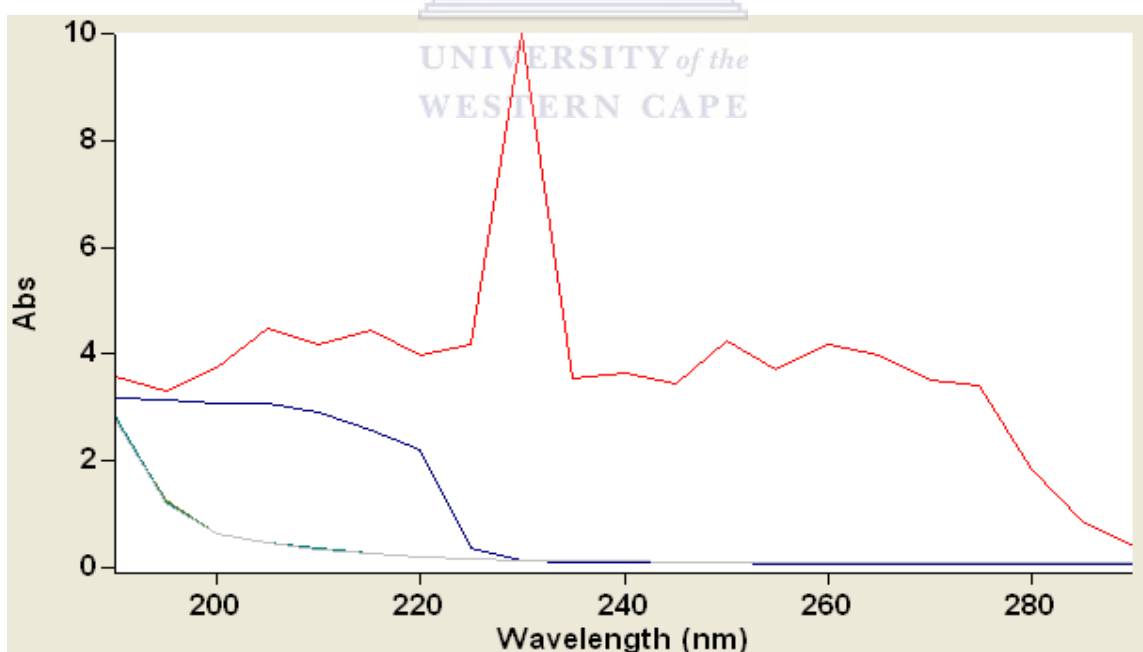


Figure 4.1.1: Absorption spectra for the NHase substrate and product.

The red, dark blue and green curves represent the calibration curves for acrylamide, acrylonitrile and the blank, respectively. Each solution contains 25 % methanol (v/v).

Adherence to the Beer-Lambert law was tested using the calibration curve shown in Figure 4.1.2. It shows hyperbolic behaviour with a distinct plateau as the acrylamide concentration approaches 10 mM.

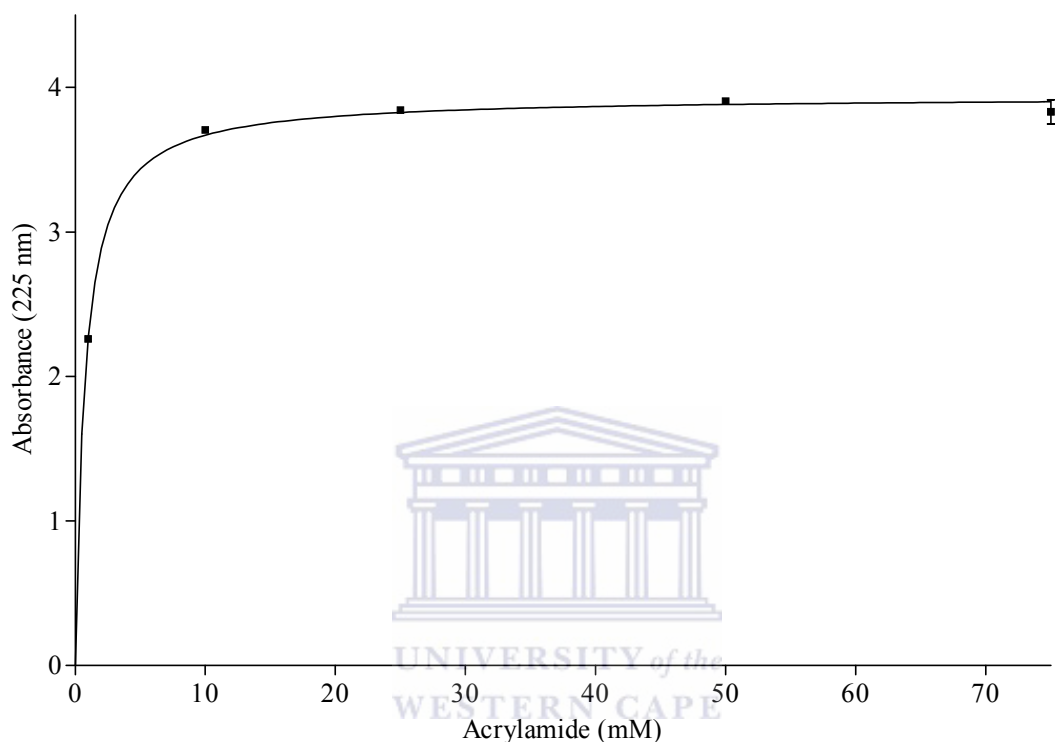


Figure 4.1.2: Calibration curve for acrylamide at 225 nm.

In order to maintain the acrylamide concentration within the linear portion of the calibration curve, it was necessary to reduce the enzyme concentration in the reaction mixture. A reduction in enzyme concentration allowed reproducible kinetic data to be obtained without the accumulation of the product concentration to levels above 1 mM.

Serial dilutions of the enzyme were used to determine an enzyme concentration that would yield a linear rate for the duration of the assay. Figure 4.1.3 is a progress curve that retains linearity between 0 and 0.6 min, using an enzyme concentration of 0.1 mg ml^{-1} .

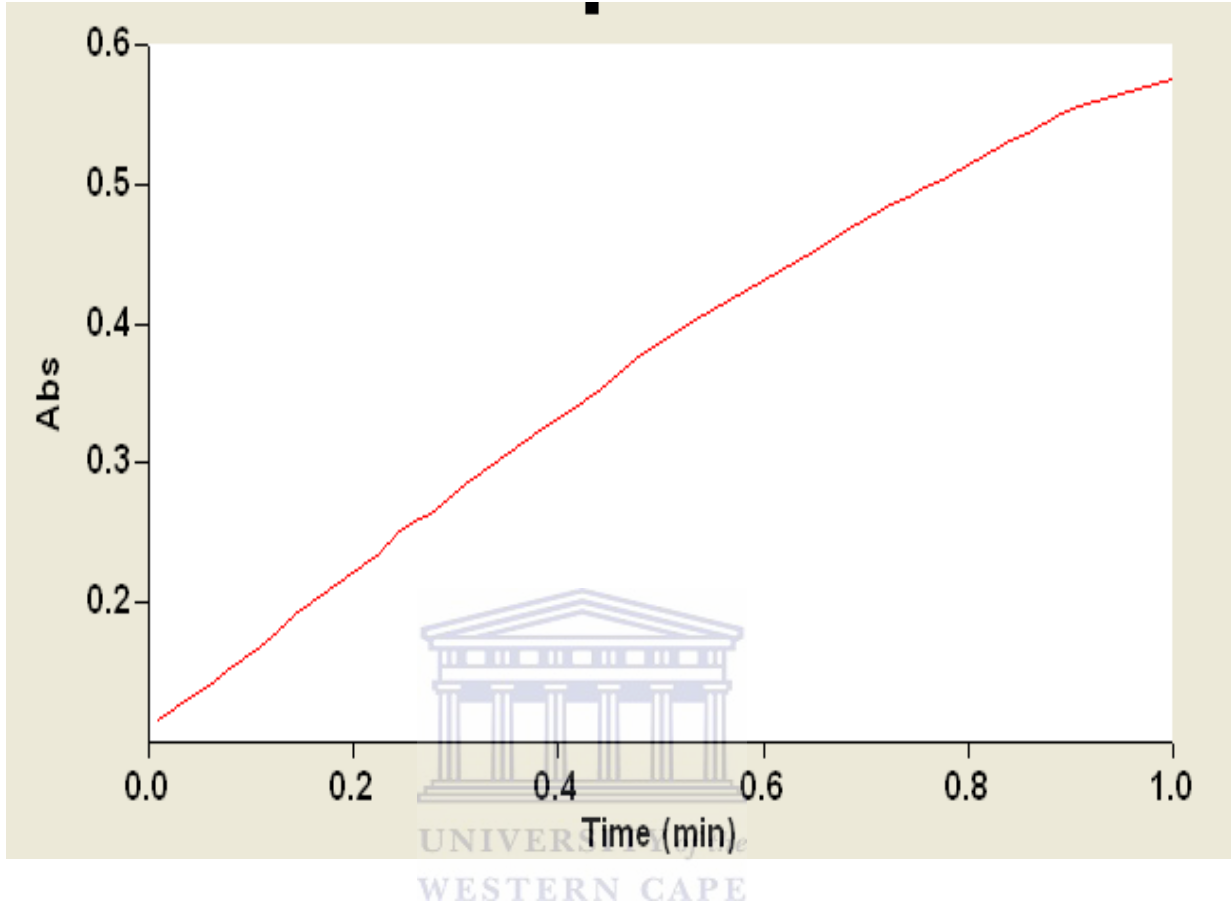


Figure 4.1.3: Absorbance vs. time plot for 0.1 mg ml⁻¹ of the β Y72F β W76V mutant NHase.

The reaction was carried out under the conditions stated in section 2.8 at a wavelength of 225 nm.

4.2 Kinetic parameters of the β Y72F β W76V mutant NHase

4.2.1 Michealis-Menten kinetics

The Michealis-Menten equation describes the relationship between the catalytic rate and the substrate concentrations. It is described as follows:

$$v_o = V_{\max} [S] / (K_m + [S])$$

where v_o is the initial velocity, V_{max} is the maximum initial velocity, K_m is the Michealis constant and $[S]$ is the substrate concentration. Figure 4.2.1 showed the graphical plot of the Michealis-Menten equation for the mutant at 50 °C and pH 7.2.

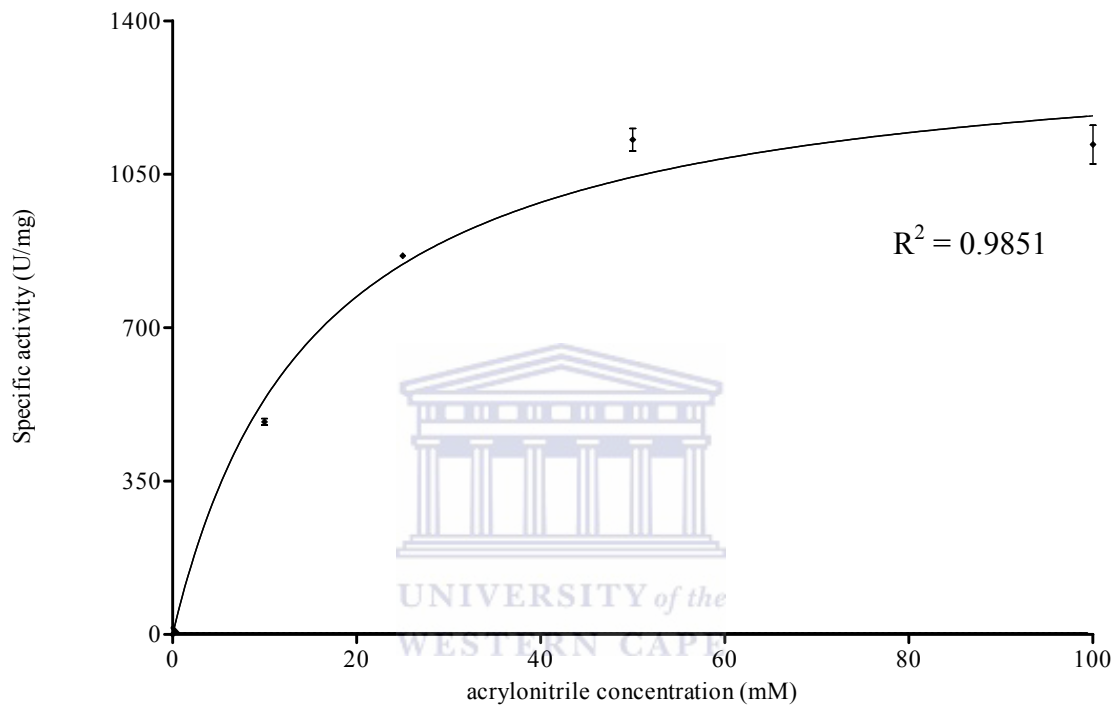


Figure 4.2.1: Michealis-Menten curve for the mutant

The upper limit of the substrate concentrations was selected on the basis that it is tenfold greater than the published wild type K_m value (Tsekoa, 2005), which gives 91 % of the theoretical rate of reaction at an infinite substrate concentration (Scopes, 1995).

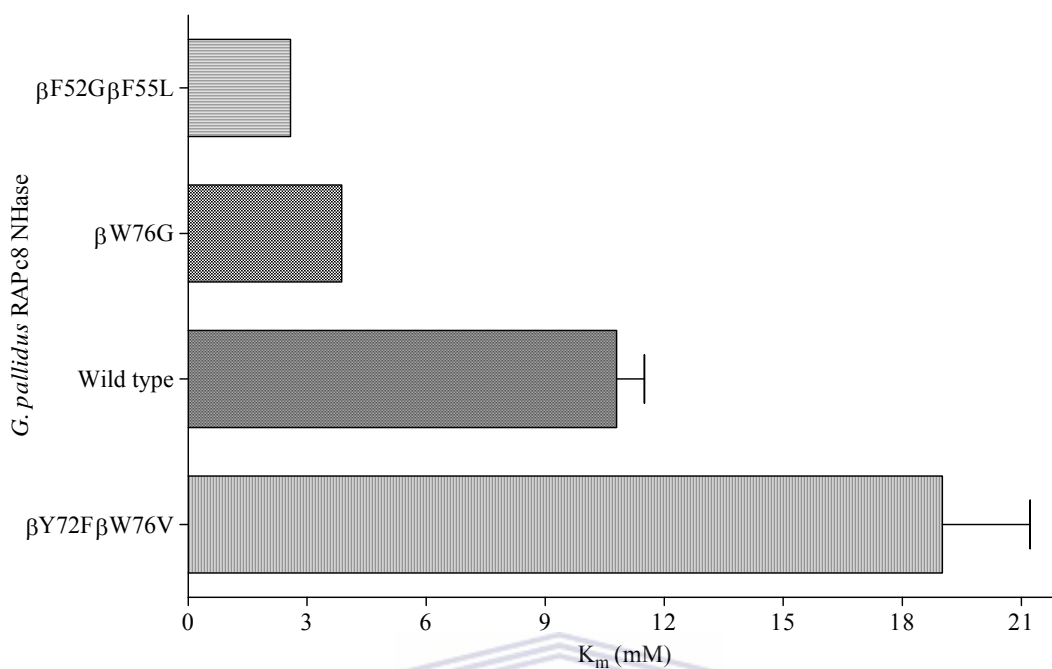
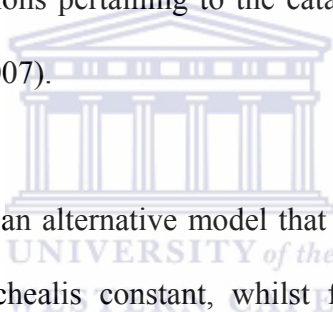


Figure 4.2.2: Michealis constants of *G. pallidus* RAPc8 NHase mutants.

The K_m and V_{max} were generated using the direct linear plot (Eisenthal and Cornish-Bowden, 1974) and calculated using the Enzpack software. The actual linear plot was not shown due to the unavailability of software capable of drawing the plot at the time of submission. Figure 4.2.2 shows the different K_m values of *G. pallidus* RAPc8 NHase mutants with acrylonitrile as the substrate. The wild type, $\beta W76G$ (Tsekoa, 2005), $\beta F52G\beta F55L$ (Kowlessur, unpublished) which correlates with the data in Tables 1.8.1 and 1.8.2, respectively, are significantly lower than the $\beta Y72F\beta W76V$ mutant. A large K_m value of the $\beta Y72F\beta W76V$ mutant indicates a lower binding affinity with acrylonitrile as compared to both of the other mutants and the wild type. However, a more valid comparison of the preference for acrylonitrile as a substrate requires the determination of specificity constants (k_{cat}/K_m).

4.2.2 Efficiency function: An alternative catalytic comparator

The validity of the k_{cat} / K_m ratio as a comparative index of substrate specificity has been discussed in detail (Eisenthal *et al.*, 2007). The use of this ratio to determine the catalytic effectiveness of enzymes will not always be valid, as two enzymes catalysing the same substrate could have identical k_{cat}/K_m value with different $[S]/K_m$ values (Eisenthal *et al.*, 2007). As $[S]/K_m$ approximates 1, k_{cat} (as opposed to K_m) becomes the determinant of catalytic efficiency. However, if the proportional difference between the k_{cat} and K_m values of two enzymes is the same, but the $[S]/K_m$ values vary, then the k_{cat}/K_m values could result in invalid conclusions pertaining to the catalytic efficiency of the enzymes under study (Eisenthal *et al.*, 2007).



The efficiency function (E_f) is an alternative model that compares the ratio between the turnover number and the Michealis constant, whilst factoring in the effects of the substrate concentration. The efficiency function takes into account the limitation imposed on catalytic activity by the rate of the diffusion of the substrate to the enzyme active site.

The rate constant of a diffusion controlled processes (k_{diff}) is approximately

$10^9 \text{ M}^{-1} \text{ s}^{-1}$ (Ceccarelli *et al.*, 2008). The equation is as follows:

$$\begin{aligned} E_f &= k_{\text{cat}} / (k_{\text{diff}}(K_m + [S])) \\ &= k_{\text{cat}} / (10^9 \text{ M}^{-1} \text{ s}^{-1} (K_m + [S])) \end{aligned}$$

When efficiency function values are plotted against the logarithm of the substrate concentration, a sigmoidal curve is obtained, as in Figure 4.2.4. This figure correlates with the data in Table 4.2.2.

Table 4.2.2: Efficiency function values of three *G. pallidus* RAPc8 NHases.

Acrylonitrile (mM)	β Y72L β W76V ($\text{mM}^{-1}\text{s}^{-1}$)	β F52G β F55L ($\text{mM}^{-1}\text{s}^{-1}$)	Wild type NHase ($\text{mM}^{-1}\text{s}^{-1}$)
0.01	1.32×10^{-4}	4.63×10^{-4}	1.82×10^{-4}
0.1	1.32×10^{-4}	4.48×10^{-4}	1.81×10^{-4}
1	1.26×10^{-4}	3.35×10^{-4}	1.68×10^{-4}
10	8.7×10^{-5}	9.5×10^{-5}	9.8×10^{-5}
100	2.1×10^{-5}	1.2×10^{-5}	1.9×10^{-5}
1000	2×10^{-6}	1×10^{-6}	2×10^{-6}

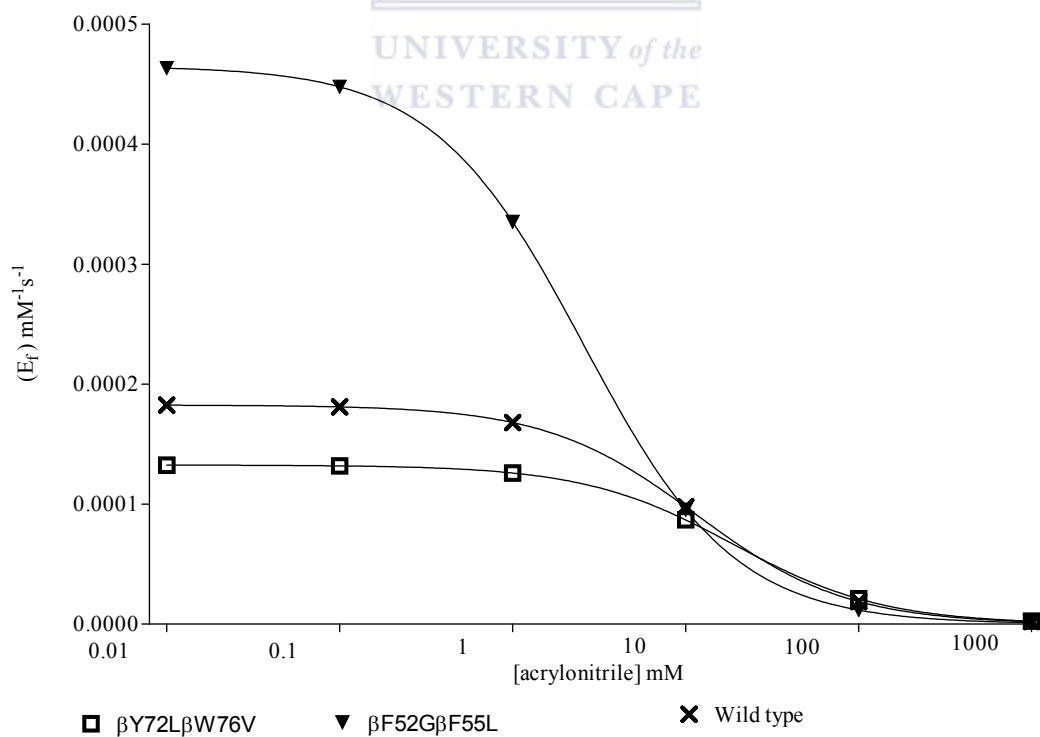


Figure 4.2.4: Efficiency function graph of the *G. pallidus* RAPc8 NHase mutants.

Table 4.2.3: Specificity constants of the *G. pallidus* RAPc8 NHases mutants

NHase	k_{cat} (s^{-1})	K_{m} (mM)	$k_{\text{cat}} / K_{\text{m}}$ ($\text{mM}^{-1}\text{s}^{-1}$)
wild type	2100.0	11.5	180.0
$\beta\text{Y72F}\beta\text{W76V}$	1260.0	19.0	70.0
$\beta\text{F52G}\beta\text{F55L}$	1200.0	2.6	450.0

Table 4.2.3 is a comparison of specificity constants which suggests that the $\beta\text{F52G}\beta\text{F55L}$ mutant is the most catalytically effective *G. pallidus* RAPc8 NHase for the conversion of acrylonitrile to acrylamide. However, E_f values shown in Table 4.2.2 and Figure 4.2.4 follows the trend defined by the specificity constants in Table 4.2.3 up to 10 mM, at which point all values are virtually identical. From concentrations of 100 mM to 1000 mM, the E_f values of $\beta\text{F52G}\beta\text{F55L}$ are almost half the values of the wild type and the $\beta\text{Y72F}\beta\text{W76V}$ values as highlighted by Table 4.2.2. This comparative index could be useful in a biotechnological context such as in nitrile bioconversion, where high substrate concentrations would be utilised.

4.3 Effect of temperature on the kinetic parameters of the *G. pallidus* RAPc8 β Y72F β W76V mutant NHase

Table 4.3.1: Kinetic parameters of *G. pallidus* RAPc8 β Y72F β W76V mutant NHase

T (K)	k_{cat} (s^{-1})	K_m (mM)	k_{cat} / K_m ($mM^{-1}s^{-1}$)
313	733.1 ± 50.9	12.9 ± 3.3	56.7 ± 3.9
318	976.7 ± 33.5	18.5 ± 2.0	52.7 ± 1.8
323	1260.0 ± 80.7	19.0 ± 3.8	66.3 ± 4.2
328	1422.5 ± 79.3	24.1 ± 3.8	59.1 ± 3.3
333	2014.2 ± 316.9	71.6 ± 21.2	28.1 ± 4.4
338	150.2 ± 25.9	25.3 ± 12.2	5.9 ± 1.0

The temperature dependence of the kinetic parameters was evaluated, as shown in Table 4.3.1.

4.3.1 Temperature dependence of k_{cat}

In determining enzyme rates at different temperatures, no activity was detected above 338 K (65°C), whilst optimal activity was detected at 333 K. Figure 4.3.1 is a plot of the natural logarithm of the turnover number against the inverse of the temperature. It follows the Arrhenius equation; $\ln k = \ln A - E_a / RT$, where k is the rate constant, E_a is the activation energy, R is the gas constant and T is the absolute temperature. This plot is consistent with the published activity profile of the wild type (Pereira *et al.*, 1998). The linear slope of the graph between 0.003 and 0.0032 (that is, the inverse of the values between 313 and 333 K) indicates the temperature independence of the rate-limiting step.

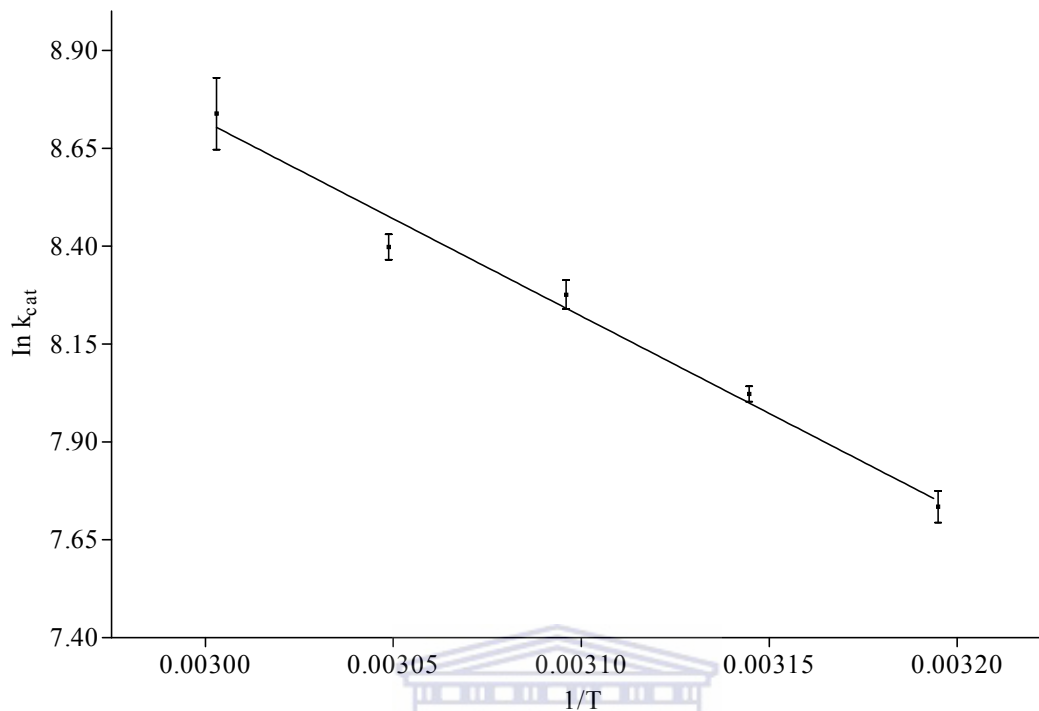


Figure 4.3.1: Linear Arrhenius plot of the *G. pallidus* RAPc8 NHase β Y72F β W76V mutant.

The activation energy was determined from the slope of the Arrhenius plot = $-E_a/R$. For temperatures between 313 and 333 K, the slope and the pre-exponential factor were determined as -4997 ± 180 and 22.6 ± 0.5 , respectively. The activation energy was calculated as 41.6 ± 1.5 kJ/mol. This is a significant rise from 33.0 kJ/mol, the value attained for the wild type enzyme (Pereira *et al.*, 1998).

4.3.2 Temperature dependence of K_m

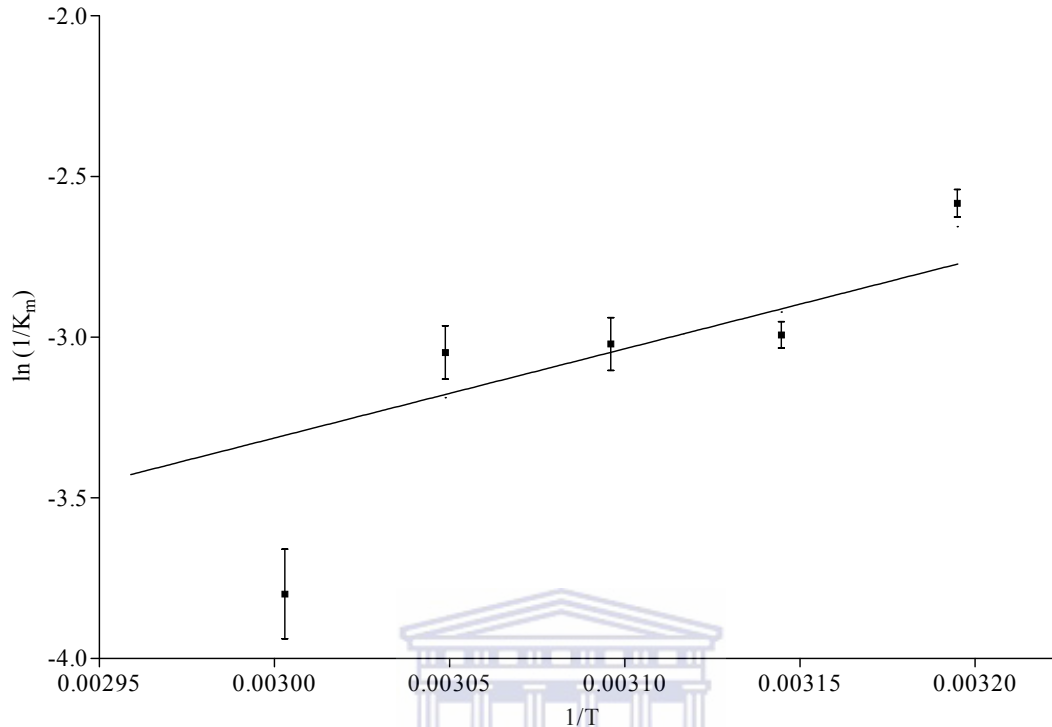


Figure 4.3.2: Plot of $\ln(1/ K_m)$ vs $1/T$ for the *G. pallidus* RAPc8 β Y72F β W76V mutant NHase

Figure 4.3.2 is a linear plot of $\ln(1/ K_m)$ vs $1 / T$. The plot highlights the unusual fluctuation in K_m at 333 K, which correlates to the second point on the graph. Although the k_{cat} appears to peak at this temperature, the stability of the enzyme is compromised, as indicated by the large K_m . The standard errors of the K_m appear to rise with temperature, possibly as a result of the presence of multiple conformational states of the enzyme. These conformations are as a result of partial denaturation taking place at temperatures below the inactivation temperature. As denaturation takes place, the weak non-covalent interactions such as hydrogen bonding that maintain the spatial arrangement of the functional enzyme are disrupted (Cornish-Bowden, 1995). This results in the incorrect positioning of the key active site residues that are involved in transition state stabilisation (Boyer, 2000).

4.3.3 Thermodynamic parameters of *G. pallidus* RAPc8 β Y72F β W76V NHase

The thermodynamic parameters were attained by the substitution of the values in the equations below:

$$\Delta H^\circ = -1 \times (\text{slope}) \times R \quad \Delta G^\circ = -RT \ln(1 / K_M) \quad \Delta S^\circ = (\Delta H^\circ - \Delta G^\circ) / T$$

$$\Delta H^\ddagger = E_a - RT \quad \Delta G^\ddagger = -RT \ln(k_{\text{cat}} h / k_B T) \quad \Delta S^\ddagger = (\Delta H^\ddagger - \Delta G^\ddagger) / T$$

where k_B , h , and R are the Boltzmann, Planck, and gas constants, respectively. The enthalpy, Gibbs free energy and entropy of activation were calculated from Figure 4.3.2.

Similarly, the enthalpy, Gibbs free energy and entropy of reaction were calculated from Figure 4.3.1. The thermodynamic parameters are shown in Table 4.3.2.

Table 4.3.2: Thermodynamic parameters of the *G. pallidus* RAPc8 β Y72F β W76V mutant, *C. testosteroni* (Rao and Holz, 2008) and *P. thermophila* (Mitra and Holz, 2006) NHase

	<i>Gp</i> NHase β Y72F β W76V	<i>Ct</i> NHase	<i>Pt</i> NHase	
	ΔG° (kJ/mol)	8.1 ± 0.9	-9.7 ± 0.5	-7.3 ± 0.4
E + S ES (activation)	ΔH° (kJ/mol)	-20.6 ± 2.2	-14.3 ± 0.5	-10.2 ± 0.5
	ΔS° (J/mol)	-88.4 ± 0.7	-10.3 ± 0.7	-9.7 ± 0.7
	ΔG^\ddagger (kJ/mol)	60.2 ± 0.5	63.2 ± 0.5	61.1 ± 1.0
ES (ES-EP) (reaction)	ΔH^\ddagger (kJ/mol)	38.9 ± 0.1	30.8 ± 0.8	18.0 ± 0.9
	ΔS^\ddagger (J/mol)	-66.2 ± 0.5	-110.4 ± 0.7	-146 ± 0.7
	E_a (kJ/mol)	41.6 ± 1.5	33.3 ± 3.5	23.0 ± 1.2

The table shows a positive Gibbs free energy of activation (ΔG°) attained for the *G. pallidus* RAPc8 β Y72F β W76V NHase as compared to the wild type NHases, suggesting that the formation of the ES complex is thermodynamically unfavourable. However, the smaller values for enthalpy and entropy of activation may significantly influence the feasibility of the reaction. A smaller enthalpy of activation relates to less intermolecular activity being required for the transition state. The entropy of activation is smaller and more negative by a factor of 9 as compared to wild type NHases. ΔS° relates to the higher probability of transition state formation due to that the ES complex is highly ordered. The small ΔS° suggests a loss of flexibility on enzyme – substrate (ES) complex formation due to hydrogen bond formation between the *G. pallidus* RAPc8 β Y72F β W76V NHase active site amino acids, water molecules and acrylonitrile (Cornish-Bowden, 1995). The more negative ΔS° value corresponds to the greater probability of spontaneous ES complex formation. The decrease in the values for entropy and enthalpy of activation suggest that the mutant has improved catalytic capabilities. The other thermodynamic parameters, such as the positive Gibbs free energy of reaction (ΔG^\ddagger) and the enthalpy of reaction are comparable to the values of wild type NHases.

4.3.4 Temperature dependence of k_{cat}/K_m

The specificity constants shown in Table 4.3.1 suggest that the best temperature for catalysis by the β Y72F β W76V mutant was 323 K (50°C). This is the optimum temperature for catalysis by the wild type enzyme (Pereira et al, 1998). The efficiency function, when used to determine the best temperature for catalysis, showed no

significant difference from 323-333 K and from substrate concentrations of 100 mM to 1000 mM. This suggests that temperature fluctuations in that range would not significantly alter the rate of catalysis at high substrate concentrations.

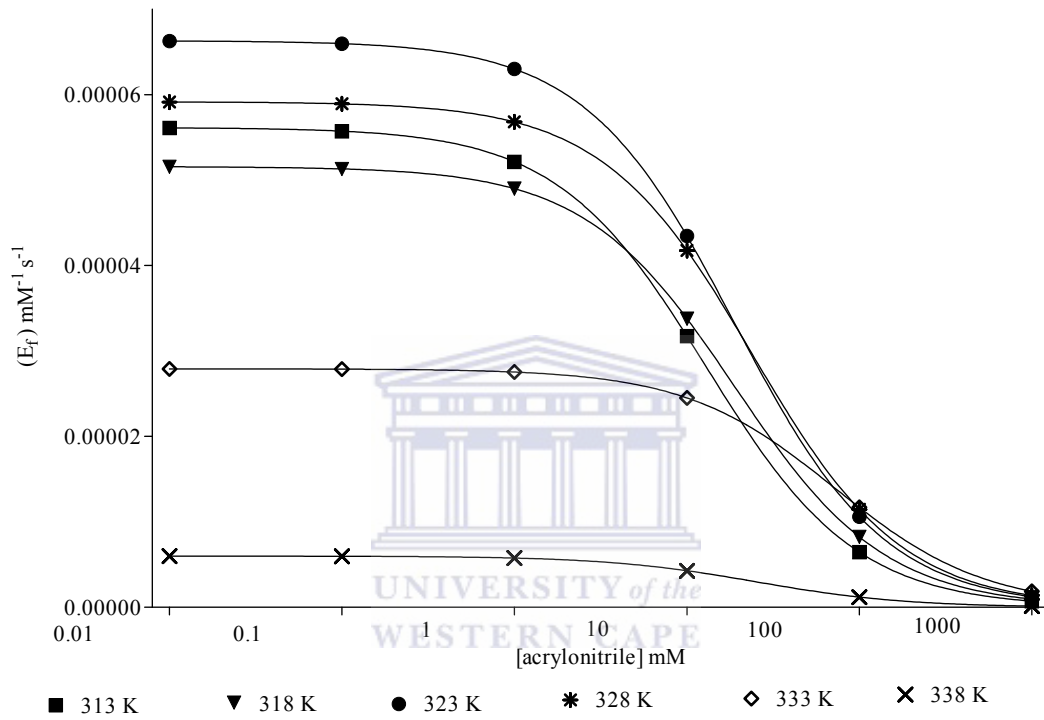


Figure 4.3.3: Variation of the *G. pallidus* RAPc8 β Y72F β W76V mutant NHase efficiency function with temperature

Table 4.3.3 Variation of the *G. pallidus* RAPc8 NHase β Y72F β W76V efficiency function with temperature

Acrylonitrile (mM)	313 K (mM ⁻¹ s ⁻¹)	318 K (mM ⁻¹ s ⁻¹)	323 K (mM ⁻¹ s ⁻¹)	328 K (mM ⁻¹ s ⁻¹)	333 K (mM ⁻¹ s ⁻¹)	338 K (mM ⁻¹ s ⁻¹)
0.01	5.6 x 10 ⁻⁵	5.2 x 10 ⁻⁵	6.6 x 10 ⁻⁵	5.9 x 10 ⁻⁵	2.8 x 10 ⁻⁵	6.0 x 10 ⁻⁶
0.1	5.6 x 10 ⁻⁵	5.1 x 10 ⁻⁵	6.6 x 10 ⁻⁵	5.9 x 10 ⁻⁵	2.8 x 10 ⁻⁵	6.0 x 10 ⁻⁶
1	5.2 x 10 ⁻⁵	4.9 x 10 ⁻⁵	6.3 x 10 ⁻⁵	5.7 x 10 ⁻⁵	2.8 x 10 ⁻⁵	5.8 x 10 ⁻⁶
10	3.2 x 10 ⁻⁵	3.4 x 10 ⁻⁵	4.3 x 10 ⁻⁵	4.2 x 10 ⁻⁵	2.5 x 10 ⁻⁵	4.3 x 10 ⁻⁶
100	6.5 x 10 ⁻⁶	8.2 x 10 ⁻⁶	1.1 x 10 ⁻⁵	1.1 x 10 ⁻⁵	1.2 x 10 ⁻⁵	1.2 x 10 ⁻⁶
1000	7.2 x 10 ⁻⁷	9.6 x 10 ⁻⁷	1.2 x 10 ⁻⁶	1.4 x 10 ⁻⁶	1.9 x 10 ⁻⁶	1.5 x 10 ⁻⁷

4.4 The effect of pH on the kinetic parameters

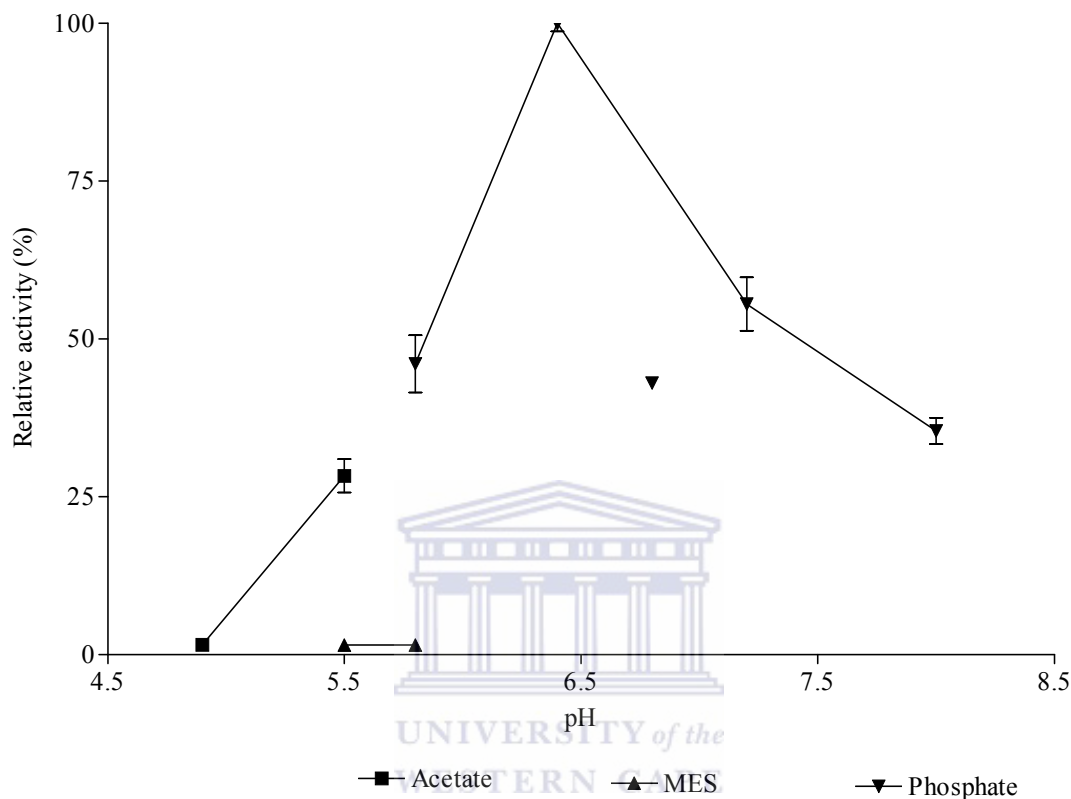


Figure 4.4.1 : pH-activity profile of the β Y72F β W76V mutant NHase

The β Y72F β W76V mutant was found to exhibit a bell shaped curve for plots of relative activity vs. pH over pH values between 4.9 and 8.0. Maximal activity was at pH 6.4. The pH optimum of the wild type was reported as 7.0, with 50 % of the relative activity at pH 5.0 and 8.7 (Pereira *et al.*, 1998). No activity was detectable at a pH of 4.2. The lack of activity at pH values below 4.8 could be attributed to destabilisation of the enzyme or a change in the ionisation of active site substrate binding residues (Pereira *et al.*, 1998).

4.4.1 Enzyme Inhibition by MES buffer

Negligible activity was detected in assays using 2-(N-morpholino) ethanesulphonic acid (MES) as a buffer. This suggests that MES may act as an enzyme inhibitor. It is noted that aromatic nitriles act as potent uncompetitive inhibitors whereas heteroaromatic substrates such as 3-cyanopyridine are excellent substrates (Tsekoo, 2005). MES is a heterocyclic amine, consisting of a heteroaromatic morpholine ring. It is interesting to note that the activity of *P. thermophila* NHase activity was unaffected by MES buffer. *P. thermophila* NHase is a Co-type NHase that was used as the enzyme in kinetics performed using benzonitrile as a substrate (Mitra and Holz, 2006). The efficacy of *P. thermophila* NHase is 100-fold higher for aliphatic nitriles than aromatic nitriles (Peplowski *et al.*, 2007). Docking studies showed substantial differences in binding modes between aliphatics and aromatics. It showed greater conformational freedom of aliphatic compounds (Peplowski *et al.*, 2007). Therefore, the inability of the *G. pallidus* RAPc8 NHase β Y72F β W76V mutant to hydrate nitriles in the presence of MES buffer may be as a result of steric hindrance caused by the bulky ring in addition to hydrophobic interactions between residues in the enzyme substrate channel and the inhibitor. The presence of a hydrophobic ring in the active site may significantly lower the diffusion rate of acrylonitrile to the active site.

4.4.2 pH dependence of kinetic parameters

Table 4.4.1: pH dependence of the kinetic parameters for *G. pallidus* RAPc8 β Y72F β W76V NHase

pH	k_{cat} (s^{-1})	K_{m} (mM)	$k_{\text{cat}} / K_{\text{m}}$ ($\text{mM}^{-1}\text{s}^{-1}$)
5.8	961.7 ± 76.7	10.2 ± 3.4	94.7 ± 7.5
6.4	2278.3 ± 144.8	26.3 ± 4.6	86.5 ± 5.5
6.8	955.8 ± 71.5	16.1 ± 4.1	59.4 ± 4.4
7.2	1260.0 ± 80.7	19.0 ± 3.8	66.3 ± 4.3
8	776.1 ± 72.8	27.2 ± 6.9	28.5 ± 2.7

Table 4.4.1 shows the variation of the kinetic parameters of the β Y72F β W76V mutant with pH. A sharp rise in the k_{cat} from pH 5.8 to 6.4 is noted, suggesting that the mutation has altered the catalytic optimum from pH 7.2, the optimum pH for the wild type NHase (Pereira *et al.*, 1998). The k_{cat} at pH 6.4 is the highest turnover rate reported for any of the *G. pallidus* RAPc8 NHase mutants (refer to Table 1.8.1). The lowest k_{cat} value is at pH 8.0. This correlates with Figure 4.4.1, a plot of the logarithm of k_{cat} against pH. However, the lowest specific activity for the mutant was recorded at pH 4.8, as shown in Figure 4.4.1. The β Y72F β W76V mutant has a k_{cat} of 1260.0 s^{-1} compared to 2100 s^{-1} for the wild type at pH 7.2. The pH optimum of the mutant is at pH 6.4 with a k_{cat} of $2278.3 \pm 144.8 \text{ s}^{-1}$.

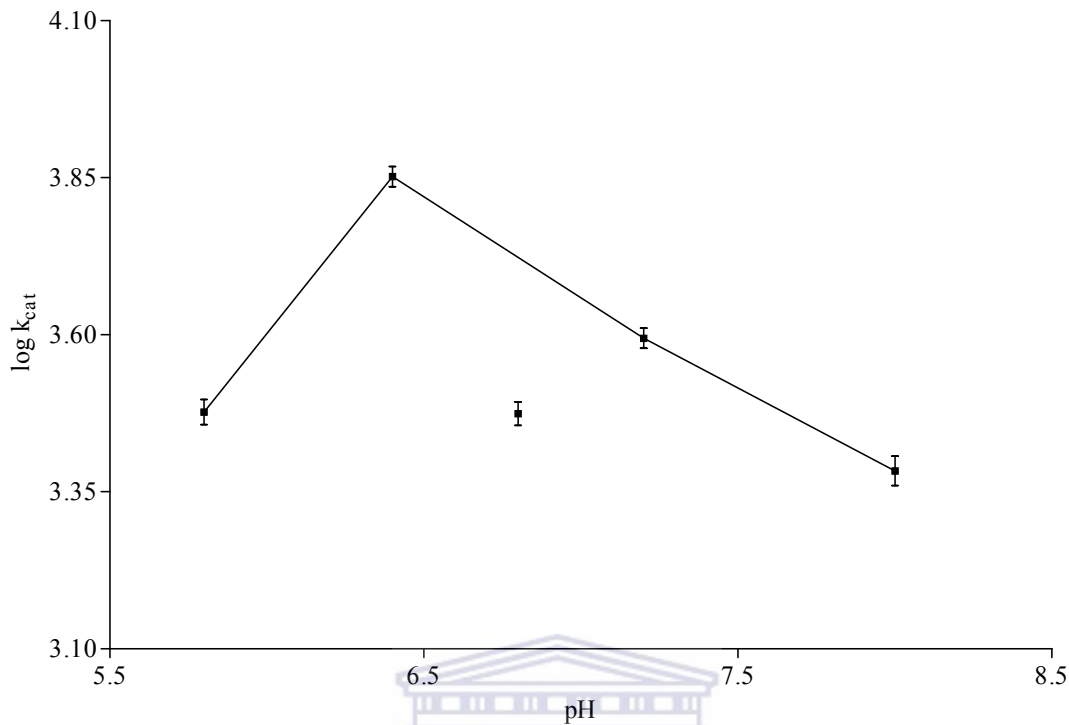


Figure 4.4.2: log k_{cat} vs pH plots of *G. pallidus* RAPc8 NHase β Y72F β W76V with acrylonitrile as the substrate.

Figure 4.4.2 is the log k_{cat} vs pH graph is similar to those in literature for *P. thermophila* (Mitra and Holz, 2006) and *Comamonas testosteroni* Ni1 (Rao and Holz, 2008) exhibiting bell shaped curve. Each slope of the bell shaped log k_{cat} vs pH curve relates to the pKa value of an ionic group. Bell shaped curves does not necessarily suggest the simplicity of the reaction mechanism. Whereas the most common assumption is that the bell curve suggests the ionisation of the enzyme and the presence of two groups in different ionic states, there are some cases in which one ionic group occupies two different ionic states (Cornish-Bowden, 1995). The drop in k_{cat} observed at pH 6.8 may suggest the presence of two bell shaped curves, suggesting the presence of four slopes of

the $\log k_{\text{cat}}$ vs pH curve, and corresponding to four ionisation states of the enzyme-substrate complex.

Table 4.4.1 shows that the K_m values fluctuating between 10 and 27 mM. This trend is shown in a $\log K_m$ vs pH graph (Figure 4.4.3) which has points scattered around the $\log K_m$ value of 1.25. The response of the experimental K_m values of *G. pallidus* RAPc8 NHase β Y72F β W76V to pH resembles the trends noted for *P. thermophila* (Mitra and Holz, 2006) and *Comamonas testosteroni* Ni1 (Rao and Holz, 2008) NHases.

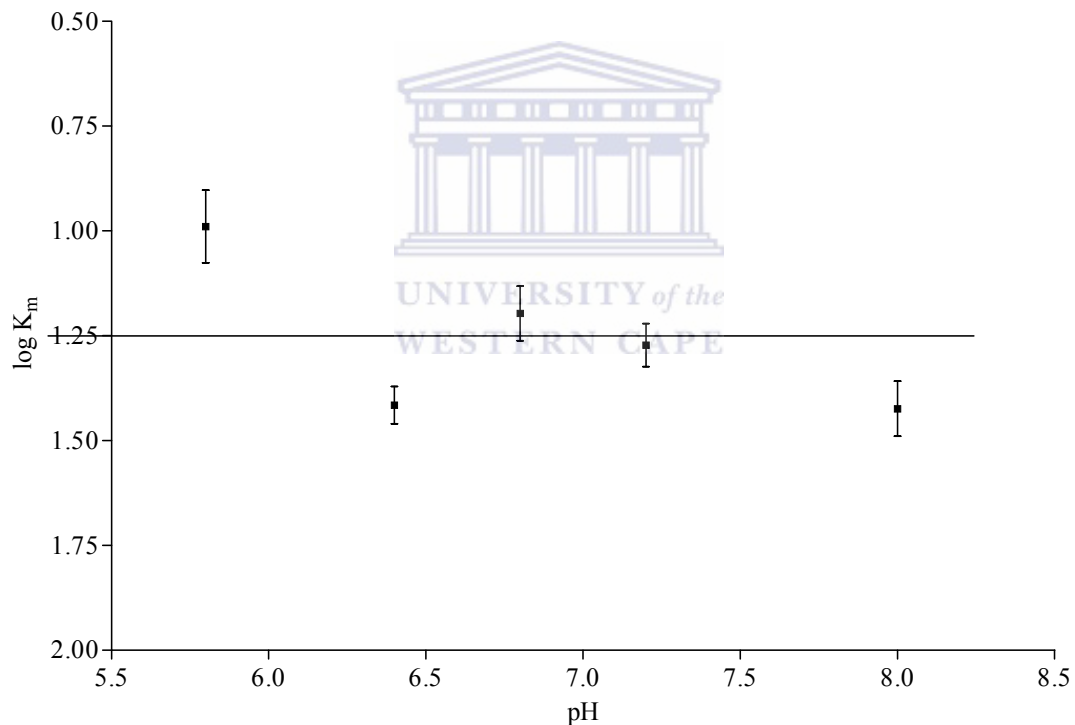


Figure 4.4.3: $\log K_m$ vs pH plot of the *G. pallidus* RAPc8 NHase β Y72F β W76V mutant with acrylonitrile as the substrate.

The general consistency in the $\log K_m$ values over the whole pH range in Figure 4.4.3 confirms that the substrate does not ionise and that the free enzyme ionisation constant values attained are not as a result of substrate ionisation. The chemical structure of

acrylonitrile renders the potential ionisation of the substrate unlikely to occur. The ionisation of the substrate would have a significant effect on substrate binding, resulting in a tangible change in $\log K_m$.

The highest $\log k_{cat} / K_m$ recorded thus far for *G. pallidus* RAPc8 NHase $\beta Y72F\beta W76V$ appears to be at pH 5.8, according to Figure 4.4.4. Broadening the range of data by testing the enzyme at lower pH values would permit meaningful conclusions to be drawn as to the left hand slope of the graph.

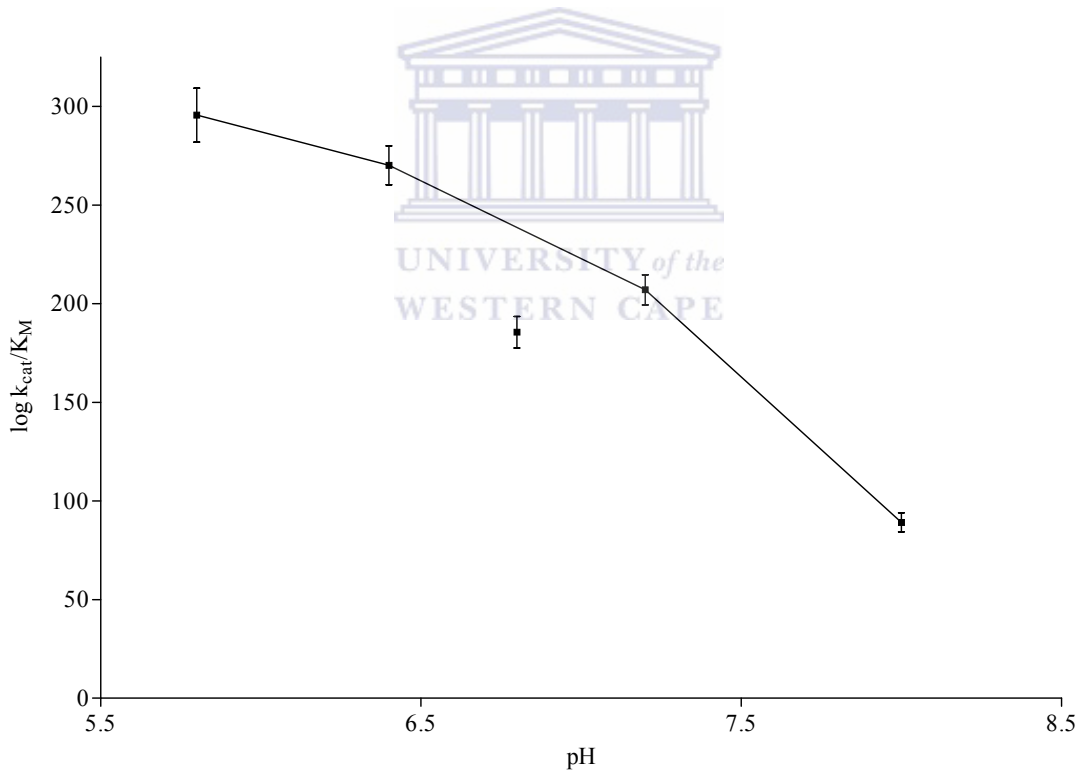


Figure 4.4.4: $\log k_{cat} / K_m$ vs pH plot of the *G. pallidus* RAPc8 NHase $\beta Y72F\beta W76V$ mutant with acrylonitrile as the substrate.

The ionisation constants can be determined by the substitution of the kinetic values into the equations below (Mitra and Holz, 2006; Rao and Holz, 2008):

$$\text{Log } k_{\text{cat}} / K_m = \log [(k'_{\text{cat}} / K_M) / (1 + ([H] / K_{E1}) + (K_{E2} / [H]))]$$

$$\text{Log } k_{\text{cat}} = \log [(k'_{\text{cat}}) / (1 + ([H] / K_{ES1}) + (K_{ES2} / [H]))]$$

(k'_{cat} = maximal turnover number, k'_{cat}/K_m = maximal value for the specificity constant)

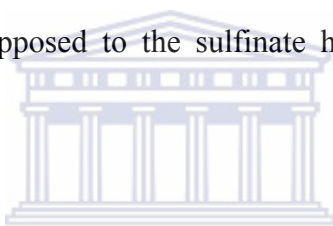
K_{ES1} and K_{ES2} are the ionisation constants of the ES complex which affect the acidic and the basic sides of the curve, respectively. K_{E1} and K_{E2} are the ionisation constants for the acidic and basic groups on the free enzyme or free ionisable substrate, respectively. The values attained are shown in the table below:

Table 4.4.2 Ionisation constants of the *G. pallidus* RAPc8 β Y72F β W76V mutant NHase

	pKa
pK_{ES1}	5.8 ± 0.1
pK_{ES2}	7.6 ± 0.1
pK_{E1}	5.5 ± 0.1
pK_{E2}	7.5 ± 0.1

Recently, it has been suggested that the pK_{ES1} of 5.9 is as a result of deprotonation of the OH group of the tyrosine amino acid or the metal coordinated sulfinic acid (Mitra and Holz, 2006). The selection of tyrosine over sulfinic acid was based on assays depicting the temperature dependence of pK_{ES1} . The allocation of a proton-shuffling role to the Y residue was in addition to a predicted putative pKa value of sulfinic acid in NHase of 7.6 (Dey *et al.*, 2006). This was also supported by the observation of a significant decrease in

$k_{\text{cat}} / K_{\text{M}}$ from 537 to $0.26 \text{ s}^{-1}\text{mM}^{-1}$ upon substituting the active site Y with F (Miyanga *et al.*, 2004). Mutation of Y68 in *P. thermophila* JCM 3095 to F68 resulted in a 126-fold decrease in the k_{cat} for acrylonitrile conversion from 1910 s^{-1} to 15.2 s^{-1} (Hopmann and Himo, 2008). For conversion of benzonitrile, the reduction of the k_{cat} of the Y68F mutant is only 17-fold. This correlated with the reduced turnover number of the *G. pallidus* RAPc8 NHase $\beta\text{Y72F}\beta\text{W76V}$ mutant compared to wild type at pH 7.2 and 50°C . However, given that the *G. pallidus* RAPc8 NHase $\beta\text{Y72F}\beta\text{W76V}$ mutant maintains the pK_{ESI} value of 5.9, then it may be probable that an alternative residue, such as the sulfinic acid suggested (Mitra and Holz, 2006) is the base involved in the hydration of nitriles. However, the sulphenate as opposed to the sulfinite has been suggested as the base responsible for NHase activity.



There are two post-translationally modified cysteine residues in the active site of NHases; the sulphinic acid (SO_2H) and the sulphenic acid (SOH). Cobalt ion coordination complexes were found to exhibit higher catalytic acetonitrile hydration activity in complexes with a monooxygenated sulphur as compared to complexes with doubly oxygenated sulphur (Heinrich *et al.*, 2004). Time-resolved X-ray crystallography of the catalytic mechanism of *Rhodococcus erythropolis* N771 NHase conversion of *tert*-butylisocyanide to *tert*-butylamine showed that the substrate was coordinated to the iron and then attacked by a water molecule activated by $\alpha\text{Cys-SOH}$ (Hashimoto *et al.*, 2008). A water molecule is activated by the $\text{O}\delta$ of $\alpha\text{114C-SOH}$ (sulphenic acid), which in turn acts as a nucleophile on the cyanide carbon of nitriles (Hashimoto *et al.*, 2008). This was

confirmed by the loss of catalytic function upon the oxidation of the sulphenic acid to sulfinic acid (Hashimoto *et al.*, 2008).

Experimental data shown in Table 4.4.2 noted a change in the pK_{ES2} from 9.2 (Mitra and Holz, 2006) to 7.6. This significant drop was unexpected as the active site S120 residue, previously implicated as the mediator of Y deprotonation (Rao and Holz, 2008), was not substituted. The identification of the residue responsible for pK_{ES2} in the mutant cannot be made without X-ray crystallographic data. Indeed, structural evidence did not show any change in the active site S and R residues of a NHase during catalysis (Hashimoto *et al.*, 2008). It is interesting to note that the pK_a value of the bound water acidified by the sulphinate complex $[Co(PyPS(SO_2)(H_2O)]^-$ was 7.2 ± 0.06 (Tyler *et al.*, 2003), which is remarkably similar to the pK_{ES2} value attained.

Efficiency functions of the pH variant kinetic parameters showed a significant difference between the efficiency of the reaction at pH 5.8 and 6.4 at substrate concentrations above 1 mM. Table 4.4.3 shows a two-fold difference between pH 6.4 E_f values as compared to the values obtained at pH 5.8 and 7.2, and a four-fold difference compared to pH 6.8 and pH 8.0. Therefore, optimisation of the catalytic activity of the *G. pallidus* RAPc8 $\beta Y72F\beta W76V$ mutant NHase could be carried out at pH 6.4.

Table 4.4.3 Variation of the *G. pallidus* RAPc8 β Y72F β W76V mutant NHase efficiency function with pH

Acrylonitrile (mM)	pH 5.8 (mM ⁻¹ s ⁻¹)	pH 6.4 (mM ⁻¹ s ⁻¹)	pH 6.8 (mM ⁻¹ s ⁻¹)	pH 7.2 (mM ⁻¹ s ⁻¹)	pH 8.0 (mM ⁻¹ s ⁻¹)
0.01	9.6 x 10 ⁻⁵	8.8 x 10 ⁻⁵	5.9 x 10 ⁻⁵	6.6 x 10 ⁻⁵	2.9 x 10 ⁻⁵
0.1	9.5 x 10 ⁻⁵	8.8 x 10 ⁻⁵	5.9 x 10 ⁻⁵	6.6 x 10 ⁻⁵	2.9 x 10 ⁻⁵
1	8.8 x 10 ⁻⁵	8.4 x 10 ⁻⁵	5.6 x 10 ⁻⁵	6.3 x 10 ⁻⁵	2.8 x 10 ⁻⁵
10	4.8 x 10 ⁻⁵	6.3 x 10 ⁻⁵	3.7 x 10 ⁻⁵	4.3 x 10 ⁻⁵	2.1 x 10 ⁻⁵
100	8.8 x 10 ⁻⁶	1.8 x 10 ⁻⁵	8.2 x 10 ⁻⁶	1.1 x 10 ⁻⁵	6.1 x 10 ⁻⁶
1000	9.5 x 10 ⁻⁷	2.2 x 10 ⁻⁶	9.4 x 10 ⁻⁷	1.2 x 10 ⁻⁶	7.6 x 10 ⁻⁷

Chapter 5: General discussion and conclusions

5.1 Summary

The main objective of this study was to study the catalytic mechanism of NHases. The method followed was based on the experimental protocol and analysis techniques used by Mitra and Holz (2006) and Rao and Holz (2008) to elucidate the reaction mechanism of NHases. Site directed mutagenesis was carried out in order to determine whether the active site Y and W residues are essential for catalysis. The enzyme was expressed in and purified from BL21 (plays) DE3 *E. coli* by heat treatment, phenyl-Sepharose (hydrophobic interaction) chromatography, Q-Sepharose (anion exchange) chromatography and shown to exhibit a single oligomeric form by gel filtration.

Kinetic assays were performed and the enzyme was studied as a model for the catalytic mechanism of NHases using acrylonitrile as a substrate. The k_{cat}/K_M ratio was significantly lower than the wild type, with a drop from $180 \text{ M}^{-1}\text{s}^{-1}$ in the wild type to $66 \pm 4 \text{ M}^{-1}\text{s}^{-1}$ in the $\beta\text{Y72F}\beta\text{W76V}$ mutant at 50°C and pH 7.2. Though the temperature optimum remained at 50°C , the activation energy had noted a 7.6 kJ/mol rise.

The pH-activity profile showed a slight drop in specific activity and turnover number at pH 6.8, a rise at pH 7.2 and then a steady drop at pH 8.0. This trend could suggest the presence of two bell curves as opposed to one. Further study is necessary to clarify this.

The pH optimum saw a significant drop from pH 7.2 in the wild type to pH 6.4 in the mutant. The turnover number was highest at pH 6.4, though the k_{cat}/K_m ratio was highest at pH 5.8. Analysis of the kinetic data yielded the ionisation constants for the enzyme-substrate complex and the free enzyme for the acidic and basic sides. The pK_{ES1} and the pK_{E1} did not change, even though the mutation substituted the active site tyrosine with a phenylalanine would be expected to significantly change the active site geometry. Since the acidic ionisation constants did not change, the oxidised cysteine residue as opposed to the tyrosine was implicated as the catalytic residue. The basic side ionisation constants changed dramatically even though the serine residue was not substituted.

Based on the experimental results attained, no direct catalytic function was noted in the active site W76 or Y72. Previous studies have shown improved binding affinity and reduced aromatic inhibition on substituting the W76 residue with a G residue (Tsekoa, 2005). The active site Y72 may have a role in the binding of the substrate to the active site. This correlates with the high K_m values attained by the *G. pallidus* RAPc8 $\beta Y72F\beta W76V$ mutant NHase, suggesting the instability of substrate binding. It was suggested that Y68 (which is homologous to Y72 in *G. pallidus* RAPc8 NHase) is not essential for NHase-mediated nitrile conversion but was probably a stabilising residue that donates a hydrogen bond to the substrate or another catalytic residue (Hopmann and Himo, 2008).

5.2 Further studies

Time dependant thermostability assays could be performed on the *G. pallidus* RAPc8 NHase mutants so as to provide valuable information as to the stability and shelf-life of the mutants. The equilibrium model of the temperature dependence of enzymes suggests that enzyme inactivation is time dependant and partially reversible (Eisenthal *et al.*, 2003). The inactivated enzyme undergoes irreversible thermal denaturation. The thermal inactivation and thermal denaturation profiles for the mutants as well as the wild type would need to be determined.

G. pallidus RAPc8 NHase does not catalyse conversion of true aromatic nitriles such as benzonitrile and benzyl cyanide (Cameron, 2002; Pereira *et al.*, 1998). Conservation of amino-acid residues L48, F51 and W72 in the NHase from *Pseudonocardia thermophila* (Miyanaga *et al.*, 2003) in relation to the low benzonitrile activity (Mitra and Holz, 2006) resulted in the selection of these residues for mutation in the *G. pallidus* RAPc8 NHase. Reduced benzonitrile inhibition in the W76G mutant (Tsekoa, 2005) and high benzonitrile activity in the β F52G β F55L (Kowlessur *et al.*, unpublished) was observed. It has been suggested that a combination of these mutations might lead to higher aromatic specificity (Tsekoa, 2005). The combination of β F52G β F55L and β Y72F β W76V may yield an efficient mutant with aromatic activity.

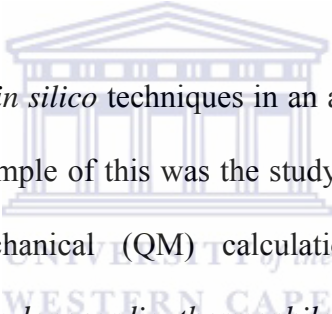
Taniguchi *et al.* (2008) identified a *Rhodococcus* sp. N771 NHase that exhibits catalytic activity with isonitriles. Isonitriles differ from nitriles in that the side chain is attached to the cyanide nitrogen in isonitriles as opposed to the cyanide carbon in nitriles. Prior to the

discovery of *Rhodococcus* sp. N771 NHase, isonitrile hydratase was the only enzyme known to hydrolyse isonitriles (Taniguchi *et al.*, 2008). Homology modelling could be performed using *Rhodococcus* sp. N771 NHase as well as other NHase molecular models to enhance the substrate specificity of the NHase. Error-prone PCR, which has been previously used to enhance NHase thermostability (Van Wyk, 2008), could be used to further engineer *G. pallidus* RAPc8 NHase to broaden the substrate specificity spectrum to include isonitriles.

Crystal trials were carried out at 20°C in 30% PEG 400, 100mM magnesium chloride, 100mM MES (2[N-Morpholino]ethanesulfonic acid), pH 6.5 (40 mg/ml NHase). This composition was previously used to generate *G. pallidus* RAPc8 NHase wild type crystals (Tsekoa, 2005), and is very similar to the composition of the conditions used to crystallise *Bacillus smithii* NHase (Hourai *et al.*, 2003). Crystals for the mutant were yet to be successfully generated. Future studies would encompass trials that involve modifying the crystallisation parameters. White crystalline precipitate in the orange solubilised NHase-buffer droplet observed indicate that the magnesium chloride concentration used may have been too high for the formation of the mutant crystal.

The effect of MES buffer on the wild type is unknown, though since the buffer inhibited the β Y72F β W76V mutant, it is likely to inhibit the wild type enzyme as well. No residual MES was observed in the substrate channel or active site of the *G. pallidus* RAPc8 NHase wild type crystal structures (Tsekoa, 2005). Inhibition kinetics could be performed

to determine the type of inhibition. Incubation of the NHase in MES followed by dialysis could be used to determine whether or not the inhibition is reversible. Reversible non competitive inhibition by MES would provide a unique opportunity to slow down the reaction and generate crystals with the substrate and product bound to it. This could be done by determining the change in the reaction rate upon the addition of different MES concentrations to the reaction mixture. Once the rate is known, it may be possible to perform time resolved X-ray crystallography as was done by Hashimoto *et al.* (2008) for the *Rhodococcus erythropolis* N771 NHase. This may confirm the role of an oxidised cysteine residue in the catalytic mechanism of nitrile hydratases.



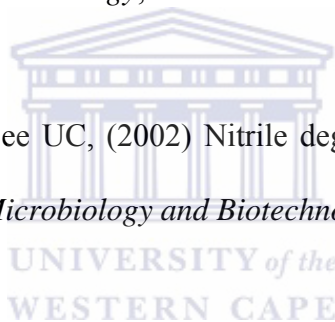
A variety of studies have used *in silico* techniques in an attempt to elucidate the reaction mechanism of NHases. An example of this was the study involving the utilisation of the semi-empirical quantum mechanical (QM) calculation method by TRITON of acrylonitrile hydration by *Pseudonocardia thermophila* JCM3095 NHase (Yu *et al.*, 2008). Though *in silico* techniques yield valuable information pertaining to the reaction mechanism, there is a need to combine such techniques with X-ray crystallography and enzymology to give a clearer picture as to how NHases work. Understanding the molecular basis for NHase-mediated catalysis could assist in the optimisation of the non-hydrolytic nitrile hydration process, rendering it useful for industrial exploitation.

References

Agarkar VB, Kimani SW, Cowan DA, Sayed M, Sewell T (2006) The quaternary structure of the amidase from *Geobacillus pallidus* RAPc8 is revealed by its crystal packing, *Acta crystallographica* section F; 62: 1174 – 1178

Banat IM, Marchant R, Rahman TJ (2004) *Geobacillus debilis* sp. nov., a novel obligately thermophilic bacterium isolated from a cool soil environment, and reassignment of *Bacillus pallidus* to *Geobacillus* comb. nov.; *International Journal of systematic and evolutionary Microbiology*; 54 : 2197 - 2201

Banerjee A, Sharma R, Banerjee UC, (2002) Nitrile degrading enzymes: current status and future prospects, *Applied Microbiology and Biotechnology*; 60 : 33 - 44



Berglund P and Park S (2005) Strategies for Altering Enzyme Reaction Specificity for Applied Biocatalysis; *Current Organic Chemistry*; 9:325-336

Bikowski TA, Naghibzadeh S, Liang J (2003) CASTp: Computed Atlas of Surface Topology of proteins; *Nucleic Acids Research*; 31 (13): 3352 - 3355

Boyer R (2000) *Modern Experimental Biochemistry*; 3rd edition; Benjamin Cummings; USA

Brady D, Beeton A, Zeevart J, Kgaje C, van Rantwijk F, Sheldon RA (2004) Characterisation of nitrilase and nitrile hydratase biocatalytic systems; *Applied Microbiology and Biotechnology*; 64: 76 - 85

Bustard MT, Whiting S, Cowan DA, Wright PC (2002) Biodegradation of high-concentration isopropanol by a solvent-tolerant thermophile, *Bacillus pallidus*; *Extremophiles*; 6: 319 – 323

Cameron RA (2002) *Nitrile degrading enzymes from extreme environments*; PhD Biochemistry and Molecular Biology thesis; University College of London

Cameron RA., Sayed M, Cowan DA (2005) Genetics and enzymology of recombinant and engineered thermostable nitrile hydratases; *Biochimica et Biophysica Acta*. 1725: 35 - 46

Ceccarelli EA, Carrillo N and Roveri OA (2008) Efficiency function for comparing catalytic competence; *Trends in Biotechnology*, 26 (3): 117-118

Cedrone F, Menez A and Quemeneur E (2000) Tailoring new enzyme functions by rational redesign; *Current Opinion in Structural Biology*; 10:405–410

Clark J M and Switzer R L (1977) *Experimental Biochemistry*; 2nd edition; W.H.Freeman and Company; New York

Cornish-Bowden A (1995) *Fundamentals of Enzyme kinetics*; revised edition; Portland Press; United Kingdom

Cowan D, Cramp R, Periera R, Graham D, Almatawah Q; (1998) Biochemistry and Biotechnology of mesophilic and thermophilic nitrile metabolising enzymes; *Extremophiles*; 2: 207 - 216

Cramp RA, Cowan DA (1999) Molecular characterization of a novel thermophilic nitrile hydratase; *Biochimica et Biophysica Acta*; 1431: 249 – 260

Dey A, Chow M, Taniguchi K, Lugo-Mas P, Davin S, Maeda M, Kovacs JA, Odaka M, Hodgson KO, Hedman B, and Solomon EI (2007) Sulfur K-Edge XAS and DFT calculations on Nitrile Hydratase: Geometric and Electronic Structure of the non-heme Iron Active Site; *Journal of the American Chemical Society*; 128, 533–541

Eisenthal R and Cornish-Bowden A (1974) The Direct Linear Plot: A NEW GRAPHICAL PROCEDURE FOR ESTIMATING ENZYME KINETIC PARAMETERS; *Journal of Biochemistry*; 139: 715-720

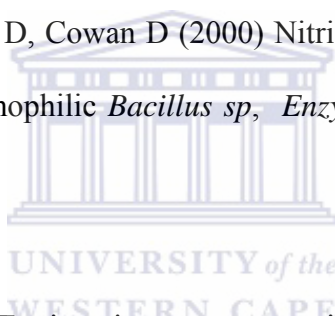
Eisenthal R, Peterson ME, Daniel RM and Danson MJ (2006) The thermal behaviour of enzyme activity: implications for biotechnology; *Trends in Biotechnology*; 24 (7): 289 – 291

Eisenthal R and Danson M J (2002) *Enzyme assays*; 2nd edition; Oxford University Press; United Kingdom

Eisenthal R, Danson MJ and Hough DW (2007) Catalytic efficiency and k_{cat}/K_M : a useful comparator?; *Trends in Biotechnology*; 25 (6): 247 – 249

Endo I, Nojiri M, Tsujimura M, Nakasako M, Nagashima S, Yohda M, Odaka M (2001) Fe-type nitrile hydratase; *Journal of Inorganic Biochemistry*; 83: 247 - 253

Graham D, Pereira R, Barfield D, Cowan D (2000) Nitrile biotransformations using free and immobilized cells of thermophilic *Bacillus sp*, *Enzyme and Microbial Technology*; 26: 368 -373



Harris JL and Craik CS (1998) Engineering enzyme specificity; *Current Opinion in Chemical Biology*; 2:127–132

Hashimoto K, Suzuki H, Taniguchi K, Noguchi T, Yohda M, and Odaka M.(2008) Catalytic mechanism of nitrile hydratase proposed by time-resolved X-ray crystallography using a novel substrate, tert-butylisonitrile; *Journal of Biological Chemistry*; in press

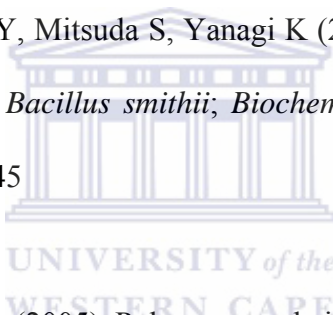
Heinrich L, Mary-Verla A, Vaissermann J, Chottard J, and Li Y (2004) Bis-axial cyanide coordination induces high nucleophilicity of the in-plane thiolato ligands bound to a Co

(III) center: model complexes related to the Co-containing nitrile hydratases ; *Inorganica Chimica Acta*; 357: 2462–2468

Hopmann KH, Guo J, and Himo F (2007) Theoretical Investigation of the First-Shell Mechanism of Nitrile Hydratase; *Inorganic Chemistry*; 46, 4850-4856

Hopmann K.H and Himo F (2008) On the Role of Tyrosine as Catalytic Base in Nitrile Hydratase; *European Journal of Inorganic Chemistry*; 3452–3459

Hourai S, Miki M, Takashima Y, Mitsuda S, Yanagi K (2003) Crystal structure of nitrile hydratase from a thermophilic *Bacillus smithii*; *Biochemical and Biophysical Research Communications*; 312: 340 – 345



Kato Y, Yoshida S, Asano Y (2005) Polymerase chain reaction for identification of aldoxime dehydratase in aldoxime- or nitrile-degrading microorganisms; *FEMS Microbiology Letters* 246 : 243–249

Kato Y, Asano Y (2006) Molecular and enzymatic analysis of the “aldoxime–nitrile pathway” in the glutaronitrile degrader *Pseudomonas* sp. K-9 *Appl Microbiology and Biotechnology*; 70: 92–101

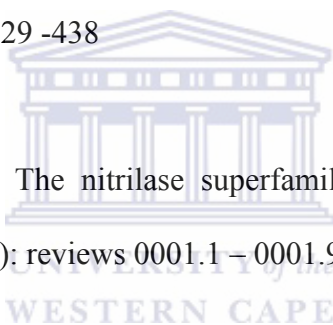
Laemmli U K (1970) Cleavage of structural proteins during the assembly of the head of bacteriophage T4; *Nature*; 227(5259):680-5

Mitra S and Holz RC (2006).Unraveling the Catalytic Mechanism of Nitrile Hydratases;
Journal of Biological Chemistry; 282(10):7397-404

Miyanga A, Fushinobu S, Ito K, Wakagi T (2001) Crystal structure of cobalt-containing nitrile hydratase; *Biochemical and Biophysical Research Communications*; 288: 1169 - 1179

Miyanga A, Fushinobu S, Ito K, Shoun H, Wakagi T (2004) Mutational and structural analysis of cobalt-containing nitrile hydratase on substrate and metal binding; *European Journal of Biochemistry*; 271: 429 -438

Pace H C, Brenner C (2001) The nitrilase superfamily: classification, structure and function; *Genome Biology*; 2 (1): reviews 0001.1 – 0001.9



Penning TM and Jez JM (2001) Enzyme redesign, *Chem. Rev*, 101: 3027-3046

Peplowski L, Kubiak K and Nowak W (2007) Insights into catalytic activity of industrial enzyme Co-nitrile hydratase. Docking studies of nitriles and amides; *Journal of Molecular Modelling*; 13(6-7):725-30

Pereira RA, Graham D, Rainey FA and Cowan DA (1998) A novel thermostable nitrile hydratase, *Extremophiles* , 2: 347 - 357

Rao S and Holz RC (2008) Analyzing the Catalytic Mechanism of the Fe-Type Nitrile Hydratase from *Comamonas testosteroni* Ni1.; *Biochemistry*. in press

Scopes RK (1994) *Protein Purification: Principles and Practice*; 3rd edition; Springer-Verlag; USA

Snell D and Colby J (1999) Enantioselective hydrolysis of racemic ibuprofen amide to s-(+)-ibuprofen by *rhodococcus* AJ270 - Structural and conformational effects in the direct enantiomeric resolution of α -methylarylacetic acid anti-inflammatory agents; *Enzyme and Microbial Technology*, 24(3) : 160-163



Taniguchi K, Murata K, Murakami Y, Takahashi S, Nakamura T, Hashimoto K, Koshino H, Dohmae N, Yohda M, Hirose T, Maeda M, Odaka M.(2008) Novel catalytic activity of nitrile hydratase from *Rhodococcus* sp. N771; *Journal of Bioscience and Bioengineering*; in press

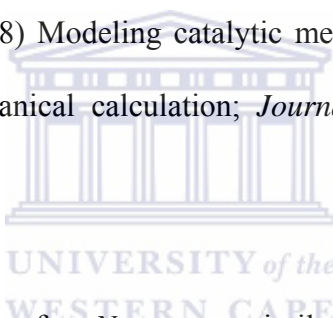
Tsekoa T, Sayed M, Sewell T, Cowan DA (2004) Preliminary structural analysis of a thermostable nitrile hydratase; *South African Journal of Science*; 100 : 488 - 490

Tsekoa T (2005) *Structure, enzymology and engineering of Bacillus pallidus RAPc8 nitrile hydratase*; PhD Biotechnology thesis; University of the Western Cape

Tyler LA, Noveron JC, Olmstead MM, and Mascharak PK (2003) Modulation of the pKa of Metal-Bound Water via Oxidation of Thiolato Sulfur in Model Complexes of Co(III) Containing Nitrile Hydratase: Insight into Possible Effect of Cysteine Oxidation in Co-Nitrile Hydratase; *Inorganic Chemistry*; 42, 5751-5761

Woodyer R, Chen W and Zhao H (2004) Outrunning Nature: Directed Evolution of Superior Biocatalysts; *Journal of Chemical education*; 81(1): 126 - 133

Yu H, Liu J, and Shen Z.(2008) Modeling catalytic mechanism of nitrile hydratase by semi-empirical quantum mechanical calculation; *Journal of Molecular Graphics and Modelling*; in press



Zeigler D.R. (2005) Application of *recN* sequence similarity analysis to the identification of species within the bacterial genus *Geobacillus*; *International journal of Systematic and Evolutionary Microbiology*; 55: 1171 – 1179

Zor T and Selinger Z (1996) Linearization of the Bradford Protein Assay Increases Its Sensitivity: Theoretical and Experimental Studies; *Analytical Biochemistry* 236: 302–308



UNIVERSITY *of the*
WESTERN CAPE